Federal University of São Carlos
Center of Exact Sciences and Technology
Physics Department

A Compact Linear Accelerator for the Production of PET Radioisotopes: Preliminary Studies

André Berretta da Costa
Undergraduate Thesis

Campinas, SP
September/2022

André Berretta da Costa

A Compact Linear Accelerator for the Production of PET Radioisotopes: Preliminary Studies

Undergraduate Thesis presented as partial requisite for the attainment of the Bachelor's Degree in Engineering Physics of the Federal University of São Carlos.
Supervisor: Prof. Dr. Fábio Aparecido Ferri

Campinas, SP
September/2022

Abstract

A compact linear accelerator will be designed for the local production of Positron Emission Tomography (PET) radioisotopes in the forthcoming Brazilian Maximum Biological Containment Laboratory (LNMCB), a biosafety level 4 (BSL-4) laboratory under construction inside the campus of the Brazilian Center for Research in Energy and Materials (CNPEM). The local production is vital to allow the use of short half-life PET radioisotopes, such as ^{11}C (20.4 min), ^{13}N (10 min), ^{15}O (2 min) and ^{18}F (110 min), for the study of highly dangerous pathogens in small animals using a hybrid PET/MR imaging system. The accelerator is under development within the framework of a collaboration agreement with the European Organization for Nuclear Research (CERN), which suggests a solution based on an innovative and very compact linear accelerator known as High Frequency Radio-Frequency Quadrupole (HF-RFQ). This solution presents several technological challenges and demands high specialized human resources, which is ideal for a frontier scientific center as CNPEM. This thesis documents part of the first efforts to understand not only theoretical and practical aspects of an HF-RFQ, but also the specific demands of the application for which the accelerator is being designed, the production of short half-life PET radioisotopes. The main routes of production of the desired radioisotopes were identified and their cross-sections curves were analysed in order to decided the most proper bombarding ion and the best output energy range for the accelerator. It was concluded by this preliminary analysis that protons accelerated up to an energy range of around 7 and 8 MeV could properly produce the short half-life PET isotopes ^{11}C, ^{13}N, ^{15}O and ^{18}F. Also, a bibliographic review of all the four existing HF-RFQ projects is presented for the purpose of gathering useful material that will help CNPEM engineers to learn from what other research groups around the world are developing.

Key-words: Compact Linear Accelerator, High Frequency Radio-Frequency Quadrupole, Production of Short Half-life PET Radioisotopes.

Resumo

Um acelerador linear compacto será projetado para a produção local de radioisótopos de Tomografia por Emissão de Pósitrons (PET) no futuro Laboratório Nacional de Máxima Contenção Biológica (LNMCB), um laboratório de Nível de Biossegurança 4 (NB-4) em construção dentro do campus do Centro Nacional de Pesquisa em Energia e Materiais (CNPEM). A produção local é vital para permitir o uso de radioisótopos PET de meia-vida curta, como ^{11}C (20,4 min), ^{13}N (10 min), ^{15}O (2 min) e ^{18}F (110 min), que serão usados no estudo de patógenos altamente perigosos em pequenos animais usando um sistema de imageamento híbrido PET/MR. O acelerador está sendo desenvolvimento no âmbito de um acordo de colaboração com a Organização Europeia para a Pesquisa Nuclear (CERN), que sugere uma solução baseada em um acelerador linear inovador e bastante compacto conhecido como Quadrupolo de Radiofrequência de Alta Frequência (HF-RFQ). Esta solução apresenta diversos desafios tecnológicos e demanda recursos humanos altamente especializados, o que é ideal para um centro científico de ponta como o CNPEM. Esta tese documenta parte dos primeiros esforços para entender não apenas os aspectos teóricos e práticos de um HF-RFQ, mas também as demandas específicas da aplicação para a qual o acelerador está sendo projetado, a produção de radioisótopos PET de meia-vida curta. As principais rotas de produção dos radioisótopos desejados foram identificadas e suas curvas de seção de choque foram analisadas a fim de decidir o íon mais adequado e a melhor faixa de energia de saída para o acelerador. Concluiu-se por esta análise preliminar que prótons acelerados até uma faixa de energia de cerca de 7 a 8 MeV podem adequadamente produzir os isótopos PET de meia-vida curta ^{11}C, ^{13}N, ^{15}O e ^{18}F. Além disso, é apresentada uma revisão bibliográfica de todos os quatro projetos de HF-RFQ existentes com o objetivo de reunir material útil que ajudará os engenheiros do CNPEM a aprender com o que outros grupos de pesquisa ao redor do mundo estão desenvolvendo.

Palavras-chave: Acelerador Linear Compacto, Quadrupolo de Radiofrequência de Alta Frequência, Produção de Radioisótopos PET de Meia-vida Curta.

Agradecimentos

Com muito prazer eu gostaria de expressar minha gratidão a todas as instituições que contribuíram para a realização dessa tese e a todas as pessoas que me apoiaram ao longo dessa jornada:

- Agradeço a minha mãe Rosângela, meu pai Luis e meu irmão Fábio. O apoio de vocês foi fundamental para a minha formação como pessoa. Se eu alcancei as conquistas que alcancei e superei os desafios que superei, foi porque existia o amparo de vocês como meu círculo familiar mais próximo.
- Agradeço ao CNPEM pela oportunidade do estágio durante o qual realizei todo o estudo, pesquisa e escrita dessa tese. Em especial, agradeço aos meus líderes Regis Terenzi e Fernando Bacchim, e também aos meus muito estimados colegas da Área de Ciências Aplicadas: Augusto, Eduarda, Isabela, Marisa, Matheus, e Tanus.
- Agradeço a UFSCar pela minha formação em Engenharia Física, curso que me proporcionou um vasto conhecimento científico sobre física, matemática e engenharia, essenciais para o desenvolvimento dessa tese. Agradeço também às dezenas de pessoas que conheci nessa instituição e que me acompanharam enquanto eu fiz parte dela como um aluno de graduação. Cada uma dessas pessoas sabe como me ajudou nessa saga e eu agradeço intensamente a cada uma delas.

Para essas e outras pessoas que me apoiaram de uma forma ou de outra ao longo da minha vida, faço uso das clássicas palavras de Carl Sagan para expressar minha gratidão por todos vocês:

"Diante da vastidão do tempo e da imensidão do universo, é um imenso prazer para mim dividir um planeta e uma época com você(s)."

Table of Contents

List of Figures . . . . . **xi**

List of Tables . . . . . **xiii**

List of Acronyms and Symbols . . . . . **xv**

1 INTRODUCTION AND CONTEXTUALIZATION **1**
1.1 Medical Radioisotopes Production **2**
1.2 Advantages of High Frequency Linacs **6**
1.3 Problem Definition and Approach **7**
1.4 Structure of the Thesis **9**

2 THEORETICAL FOUNDATIONS **11**
2.1 Radioisotope Production by Activation **11**
2.1.1 Nuclear Reaction Notation 11
2.1.2 Activity of a Radioactive Sample 12
2.1.3 Activation Cross-Section 13
2.1.4 Activation Rates 13
2.2 Radio-frequency Linacs **14**
2.2.1 Common Linac Structures 14
2.2.2 Relativistic Particles in Electromagnetic Fields 17
2.2.3 Maxwell's Equations and EM Fields in Resonant Cavities 18
2.3 The Radio-frequency Quadrupole **19**
2.3.1 Potential Function in an RFQ Cell 21
2.3.2 Longitudinal Beam Dynamics 23

3 ION BEAM SPECIFICATION FOR PET RADIOISOTOPES PRODUCTION **25**
3.1 Carbon-11 . . . . . **26**
3.2 Nitrogen-13 . . . . . **27**
3.3 Oxygen-15 . . . . . **27**
3.4 Fluorine-18 . . . . . **28**
3.5 Conclusion **29**

4 THE HIGH-FREQUENCY RFQ LINACS **31**
4.1 HF-RFQ for LIGHT by CERN/ADAM **31**
4.2 PIXE-RFQ for MACHINA Project by CERN/INFN **34**
4.3 Carbon-RFQ for Bent Linac by CERN/CIEMAT **35**
4.4 RFQ for Linac 7 by UPV/TEKNIKER/Egile **37**
4.5 Conclusion **38**

5 GENERAL CONCLUSION **39**

REFERENCES 41

List of Figures

Figure 1 – State of the art commercial cyclotron accelerator (Cyclone-IKON by IBA). . . . 3
Figure 2 – Proposed cyclotron-based facility for the production of medical radioisotopes. . . . 3
Figure 3 – Layout of PET Radioisotope Production Linac by AccSys Technology Incorporation. . . . 4
Figure 4 – Layout of in-hospital PET facility proposed by AccSys Technology Incorporation. . . . 5
Figure 5 – Mobile PET Isotope Production System by AccSys Technology. . . . 5
Figure 6 – Bombarding of a thin target material by a particle beam. . . . 13
Figure 7 – Concept of the Wideröe's drift-tube linac. . . . 15
Figure 8 – Concept of the Alvarez Drift-Tube Linac. . . . 15
Figure 9 – Structure of the side-coupled linac. . . . 16
Figure 10 – Cross section of a superconducting cavity. . . . 16
Figure 11 – Normalized velocity in function of kinetic energy for proton and suited linac structures. . . . 17
Figure 12 – TE_{110} and TE_{210} modes in a cylindrical empty cavity. . . . 19
Figure 13 – Four-vane RFQ accelerator section representation. . . . 20
Figure 14 – Modulation of the RFQ unit cells. . . . 20
Figure 15 – Visualization of the two-term potential function in a RFQ cell. . . . 22
Figure 16 – Separatrix and potential well. . . . 24
Figure 17 – Cross section for the ^{14}N(p,α)^{11}C nuclear reaction. . . . 27
Figure 18 – Cross section for the ^{16}O(p,α)^{13}N nuclear reaction. . . . 27
Figure 19 – Cross section for the ^{15}N(p,n)^{15}O nuclear reaction. . . . 28
Figure 20 – Cross section for the ^{18}O(p,n)^{18}F nuclear reaction. . . . 28
Figure 21 – Transverse cross-section and CAD of a 50 cm module of the HF-RFQ. 32
Figure 22 – Phase, aperture and modulation along the HF-RFQ for LIGHT project. 32
Figure 23 – Cell of 750 MHz IH DTL and graph of 3D envelopes, transmission and kinetic energy through it. . . . 33
Figure 24 – Completely machined HF-RFQ for the project LIGHT. . . . 33
Figure 25 – Measured and expected phase space plots of the beam after the HF-RFQ. . . . 34
Figure 26 – CAD model and cavity cross-section of PIXE-RFQ. . . . 34
Figure 27 – Some thermal and phase space simulation results of PIXE-RFQ. . . . 35
Figure 28 – Bent linac structures and energies. . . . 36
Figure 29 – CAD model of the two Carbon-RFQ cavities RFQ1 and RFQ2. . . . 36
Figure 30 – Field map of transfer path between RFQ1 and RFQ2 of the Carbon-RFQ. . . . 36
Figure 31 – Trapezoidal cells and Beam Dynamics parameters. . . . 37
Figure 32 – Cross-section and module of the RFQ for Linac7. . . . 37

List of Tables

Table 1 – PET radioisotopes production reactions. 26
Table 2 – Summary of energy demands for selected PET radioisotopes production using protons. 29
Table 3 – Summary of 750 MHz RFQ projects. 38

List of Acronyms and Symbols

The following lists summarize the meaning of acronyms and symbols used along the text of this monograph.

Acronyms

AccSys Accelerator Systems

BLS-4 Biosafety Level 4 (Maximum Biosafety Level)

CERN European Organization for Nuclear Research

CFSA Carrier-Free Specific Activity

CNPEM Centro Nacional de Pesquisas em Energia e Materiais, which translates to Brazilian Center for Research in Energy and Materials

DTL Drift Tube Linac

HF-RFQ High-Frequency Radio-Frequency Quadrupole

IBA Ion Beam Applications

LANL Los Alamos National Laboratory

Linac Linear Accelerator

LNMCB Laboratório Nacional de Máxima Contenção Biológica, which translates to Brazilian Maximum Biological Containment Laboratory

MR Magnetic Resonance

PET Positron Emission Tomography

RF Radio-frequency

RFQ Radio-Frequency Quadrupole

SCL Side-Coupled Linac

SPECT Single-Photon Emission Computed Tomography

TE Transverse Electric Mode

TM Transverse Magnetic Mode

Symbols

α	-	Alpha Particle

β	-	Normalized Velocity
β	-	Positron
$\boldsymbol{B}$	$\mathrm{N\,s/C/m}$	Magnetic Field Flux Density
$\boldsymbol{D}$	$\mathrm{C/m^2}$	Electric Field Flux Density
$\boldsymbol{E}$	$\mathrm{N/C}$	Electric Field
$\boldsymbol{F}$	N	Force
$\boldsymbol{H}$	$\mathrm{C/m/s}$	Magnetic Field
$\boldsymbol{J}$	$\mathrm{C/m^2/s}$	Current Density
$\boldsymbol{n}$	m	Boundary Normal Vector
$\boldsymbol{r}$	m	Position Vector
Δx	m	Thin target thickness
γ	-	Relativistic Mass Factor
λ	$\mathrm{s^{-1}}$	Decay Constant
λ	m	Wavelength
∇	$\mathrm{m^{-1}}$	Nabla Operator
ω	$\mathrm{rad/s}$	Radial Frequency
Φ	$\mathrm{N\,m/C}$	Electrostatic Potential
ϕ	$\mathrm{particle/m^2/s}$	Particle Beam Flux Density
ϕ_s	rad	Synchronous Phase
ρ	$\mathrm{C/m^3}$	Mass
σ	barn	Activation Cross-section
A	Bq	Activity
a	$\mathrm{Bq/g}$	Specific Activity
c	$\mathrm{m/s}$	Speed of Light
E	MeV	Kinetic Energy
k	$\mathrm{m^{-1}}$	Wavenumber
m	g	Mass
m_0	kg	Rest Mass
N	-	Number of atoms

N_{av}	mol^{-1}	Avogadro's Constant
p	kg m/s	Momentum
q	C	Charge
t	s	Time variable
$T_{1/2}$	s	Half-life Time
v	m/s	Velocity
W	MeV	Kinetic Energy
d	-	Deuteron
n	-	Neutron
p	-	Proton
A	g/mol	Mass number
a	m	Aperture
m	$-$	Modulation Factor

1 Introduction and Contextualization

The Brazilian Maximum Biological Containment Laboratory (LNMCB) will be the first biosafety level 4 (BSL-4)[1] laboratory in Latin America. Designed to be a Virology Center for *in vivo* researches using small animals, such as mice, it will also be the first BLS-4 laboratory connected to a source of synchrotron light, Sirius, which is a 4th generation synchrotron light source working inside the campus of the Brazilian Center for Research in Energy and Materials (CNPEM) [3, 4]. Three beamlines from Sirius will be employed in molecular, cellular, and morphological level researches of highly dangerous pathogens.

As a complementary research instrument to the synchrotron radiation experiments, also will be installed in the LNMCB an imaging equipment that combines Positron Emission Tomography (PET[2]) and Magnetic Resonance (MR), technically referred as a hybrid PET/MR system [6]. However, PET is an imaging technique that requires tiny amounts of certain positron decaying radioisotopes to be injected into the body of the small animals under study. And, due to the radioactive decay, the use of radioisotopes is a time-sensitive problem. Therefore, they must be acquired with certain regularity and transported as fast as possible. CNPEM has interest in short half-live radioisotopes (around seconds or minutes), but they are a particular challenge because they must be produced very near to the PET system, in order to facilitate their application while their activity is high enough to produce good quality images.

CNPEM could regularly purchase PET radioisotopes from external suppliers, which usually produce them using cyclotron accelerators, but this alternative would not favor the use of short-life PET isotopes. On the other hand, the Center has recently signed a collaboration agreement with the European Organization for Nuclear Research (CERN) that allows collaborative researches and knowledge sharing in any mutual fields of interest, specially accelerator physics, magnets, and superconducting materials [7]. Within this framework, one of the first CERN-CNPEM collaborative projects concerns a program to research and develop innovative solutions for medical radioisotope production in Brazil. CERN experts suggest a solution based on novel and very compact linear accelerator (linac) known as High Frequency Radio Frequency Quadrupole (HF-RFQ). Therefore, both sides decided that a possible and good starting point for this collaboration is the development of a linac for the local production of PET radioisotopes in the LNMBC, specially because it would benefit the use of short half-life PET isotopes, such as ^{11}C (20.4 min), ^{13}N (10 min), ^{15}O (2 min) and ^{18}F (110 min).

Within that context, this thesis has the main purpose of documenting part of the preliminary studies for the development of a high frequency linac that will locally produce radioisotopes and supply the hybrid PET/MR imaging system for small animals inside the forthcoming Brazilian BLS-4 laboratory. The three following sections provide further context about the scenario of radioisotopes production, the

[1] For more information about BLS-4 labs, check the references [1, 2].

[2] Check the reference [5] for basic explanations about Positron Emission Tomography.

advantages that a high frequency liner accelerator would have within that scenario, a better definition of the problems and challenges of the project, and the plan to approach them. The last section summarizes the content and structure of this thesis.

1.1 Medical Radioisotopes Production

There are two main imaging techniques based on the injection of radioactive material in living organisms. They differ from one another in the type of radioactive decay of the injected material. The Single Photon Emission Computed Tomography (SPECT) is a technique that uses a gamma camera to detect gamma rays directly emitted by gamma-emitting radioisotopes. Likewise, the Positron Emission Tomography (PET) uses a similar camera to detect the gamma photons emitted by the annihilation of electrons with positrons emitted by positron-emitting radioisotopes. Both imaging techniques are important parts of what is known as Nuclear Medicine[3]. The radioisotopes applied in these techniques are usually referred as Medical Radioisotopes.

Medical radioisotopes can be produced in nuclear reactors and particle accelerators. The production is possible by nuclear fission or by activation, two similar nuclear physics phenomenons. Fission fragments of heavier atoms are byproducts of nuclear reactors, and some of them can be extracted to be applied as medical radioisotopes. Nuclear reactors can also produce medical radioisotopes by a process called neutron activation, where some specific material, called target, is bombarded by neutron beams that convert part of the target nuclides into radioactive isotopes of interest. However, nuclear reactors are complex, robust and expensive facilities that require high safety protocols to be installed. For that reason, this kind of facility is not built specifically for medical radioisotopes production, but rather for several other applications [9]. Those applications generate radioactive waste from which the medical radioisotopes are extracted as byproducts. Yet, a large portion of the global radioisotope supply relies on nuclear reactors. This dependence caused a severe crisis in 2009 and the following years, when some of the main isotope supplier nuclear reactors went through series of interruptions due to aging infrastructure. Since then, innovative ways are being explored to diversify the sector of medical radioisotopes production beyond nuclear reactors [10, 11].

Fortunately, there are other interesting medical radionuclides that can be produced by activation using charged particles instead of neutron beams.[4] Some examples of charged particles that can be accelerated for that purpose are electrons, protons, deuterons, tritiums, helium-3, and alphas. Protons are the most common charged particles used in the production of low energy PET radionuclides by activation, and cyclotron accelerators are the conventional and well-established solution to accelerated them. Linacs could also be applied for the same purpose, but cyclotron accelerators have historically dominated the market because they could perform with better space and cost efficiency than usual linacs. But recently cyclotron vendors have been adopting a business model that consists of offering relatively low entry prices followed by

[3] For more information about Physics in Nuclear Medicine, check the reference [8].

[4] Theoretical basis about radioisotope production by activation are presented on Section 2.1 of this thesis.

frequent necessary maintenance, from which most of the profit comes. Cyclotrons have the disadvantage of having a considerable emission of radiation caused by beam particle losses that activate the material of the accelerator itself, demanding heavy radiation shielding around the accelerator structure. Additionally, working hours are wasted waiting for the reduction of the radiation levels before any inspection inside the shielding. Last but not least, in addition to the robust shielding infrastructure, the weight of the magnets of a cyclotron is often used as an argument in opposition to this technology.

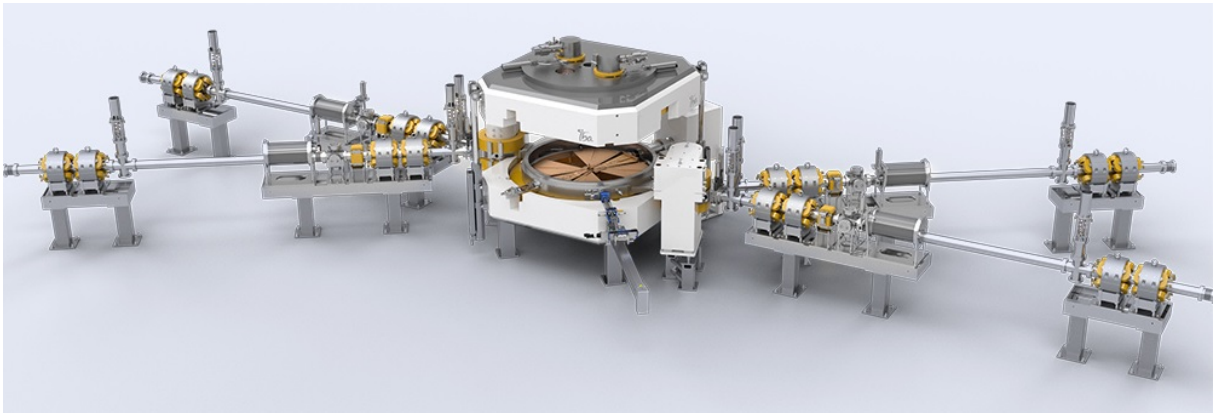

Figure 1 – State of the art cyclotron accelerator Cyclone-IKON commercialized by IBA Radiopharmasolutions. The accelerator can produce proton beams of 400 μA in the range of 13-30 MeV. [12]

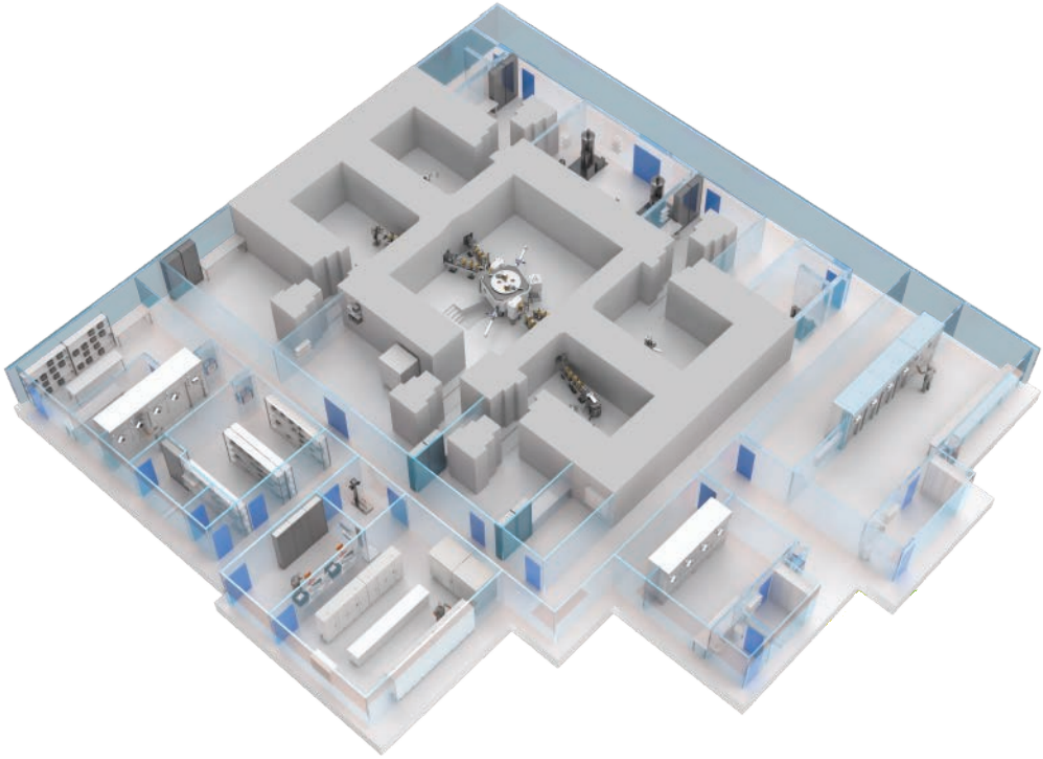

Figure 2 – 3D model of a proposed facility for the production of medical radioisotopes using the Cyclone-IKON by IBA. [13]

Even though cyclotron accelerators can successfully produce low energy medical radioisotopes, new solutions are still being proposed for the diversification of the sector. One of the most promising solutions are the High Frequency Linacs, which have the potential to overcome problems of conventional radio-frequency (RF) linacs[5] and make use of more recent technologies to properly produce medical radioisotopes with better space, cost efficiency and flexibility than cyclotrons.

The idea of employing linacs to produce medical radioisotopes goes back to the early 1980's and is somehow intimately connected to the history of a particular type of linac technology, the Radio Frequency Quadrupole (usually referred as RFQ[6]). Although research linacs were commercially producing radionuclides for medical applications by that time [14, 15], the first commercial linac for this purpose was the New England Nuclear Corporation's 45 MeV proton linac, constructed around 1981 [16, 17]. In the same year at Los Alamos National Laboratory (LANL), a 70 MeV proton linac were the first radioisotope-production linac designed with the recently demonstrated RFQ module. Meanwhile New England Nuclear's linac accelerated protons to almost half of LANL's linac, they had almost the same total length, respectively, 25.6 m and 27.3 m. These values demonstrate how RFQ modules reduced the total length of linacs.

Once the door for shorter linacs were opened, the AccSys Technology Incorporation promptly took the next step and designed a compact proton linac for in-hospital production in 1986 [18]. Designed to reach 10 MeV for the production of PET radioisotopes, AccSys Technology's compact linac could accelerate ∼25 mA through a total length of only 4.8 m. The layout of AccSys Technology's compact accelerator and the proposed medical radioisotope production facility are shown in Figures 3 and 4. After the success of this project, the company launched a modern model called PULSAR PET Isotope Production System, that was marketed at least until 2008 [19]. Even a mobile version of the product was available, in which the whole accelerator system was fit inside a 14-meter-long trailer, shown in Figure 5.

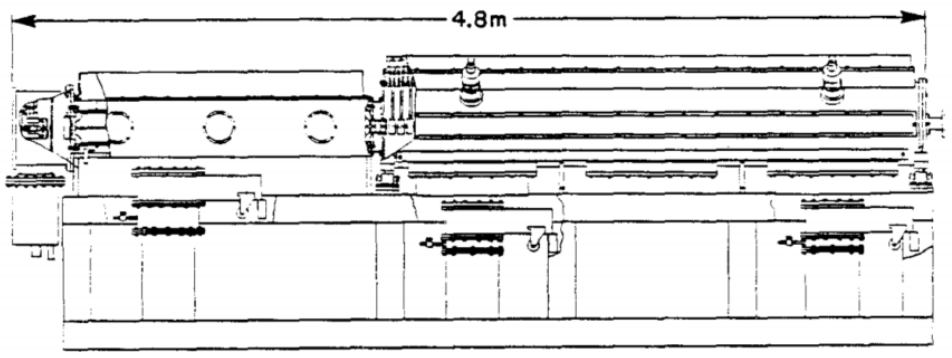

Figure 3 – Layout of PET Radioisotope Production Linac by AccSys Technology Incorporation. The proton beam is accelerated by a 1.6 meter RFQ section up to 2 MeV and then by a 2.8 meter DTL section up to 10 MeV. [18]

[5] Basic concepts of radio-frequency linear accelerators are presented on Section 2.2 of this thesis.
[6] Theoretical basis on Radio-frequency Quadrupole are presented on Section 2.3 of this thesis.

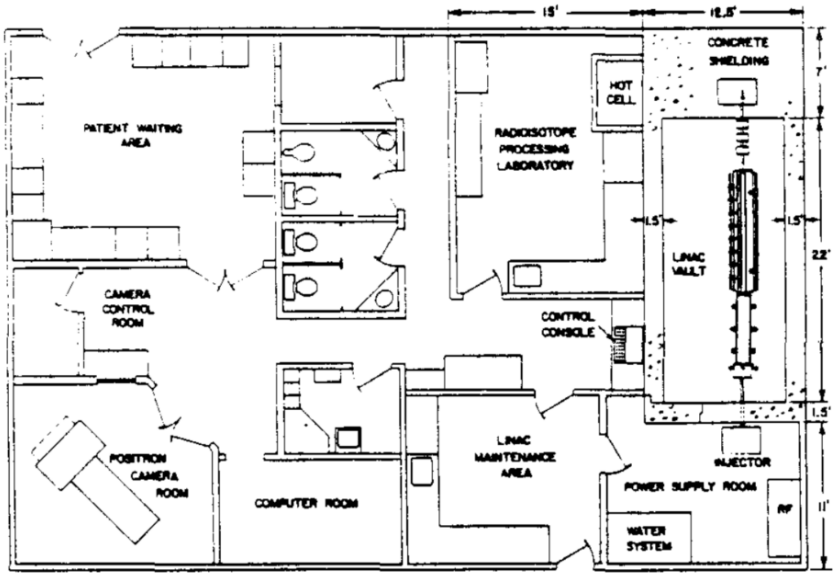

Figure 4 – Layout of PET facility proposed by AccSys Technology Incorporation as a model for an in-hospital production. [18]

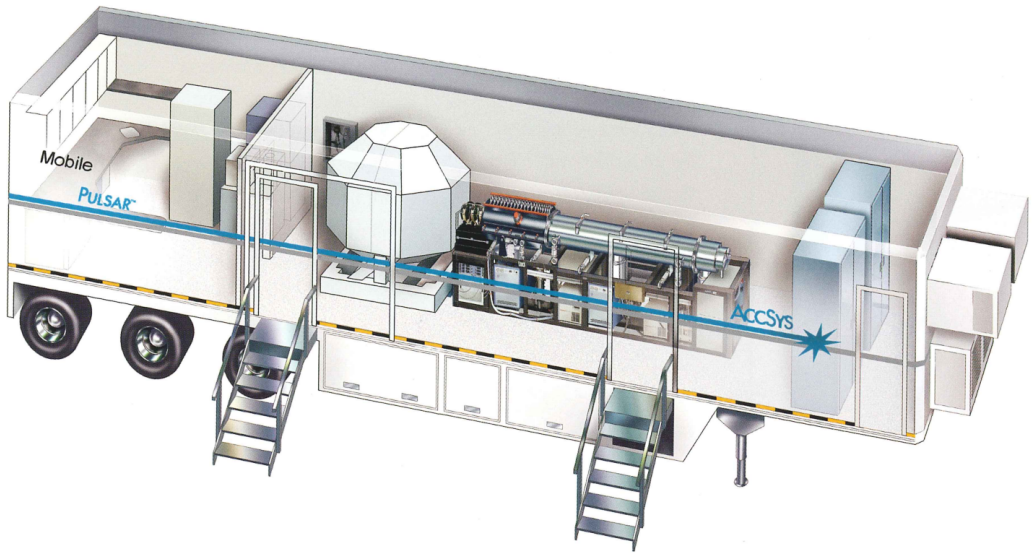

Figure 5 – Mobile PULSAR - PET Isotope Production System marketed by AccSys Technology. The whole system was fit inside a 14-meter-long trailer. [20]

However, the company is not currently offering this product and has no intention of restarting production. According to them, the market was not large enough to justify having a product line to support linacs for PET isotope production. Others argument that the end of this project is better justified by the low reliability of the RF power amplifier adopted by them, which is based on parallel planar triode arrays [21]. Despite of this, the boldness and qualities of AccSys Technology's project do not have to be wasted. Instead, new technologies like solid state based RF amplifiers and higher resonating frequencies are being proposed by CERN experts to improve the properties of old radioisotope linac projects, turning them into competitive alternatives on the market.

1.2 Advantages of High Frequency Linacs

One of the main design specifications of an RF powered linac is the frequency of the electromagnetic radiation that resonates inside the accelerator cavity and accelerates the ions. Resonating frequencies are determined by the geometry and dimensions of the cavity. For this reason, linacs working on higher resonating frequencies have smaller and shorter cavities, and are useful for applications in which compactness matters, like medical applications. Also, smaller cross sections and shorter linacs mean lower costs because of less material requirement.

However, because of the spatial limitation and the repulsion effects between the ions into the beam, higher frequency linacs accelerate lower currents than the conventional linacs. Unfortunately, even working with lower currents, the power requirements are still similar to conventional linacs, which is still a key issue that rises the costs of this type of accelerator.

An RFQ linac is capable of bunching, focusing and accelerating charged particles with high reliability. It can be designed to reach low beam losses and good beam quality, even promising to dismiss radiation shielding, sparing considerable space of the total system. This type of linac have recently been studied for medical applications that demand low current beams in the form of particle bunches with energies around 5 MeV. An RFQ linac working on a high frequency is a novel alternative and its medical and industrial applications are still being explored, but it promises compactness, no radiation shielding, versatility, and low maintenance. Those are the main arguments that concern the technology patented and made available by CERN experts called High Frequency Compact Linac [22, 23]. It consists of an RFQ working at 750 MHz, composed by 50 cm modules with an external diameter of 13.4 cm.

Some advantages and limitations of the high-frequency compact RFQ proposed by CERN for low energy and low current beams are summarized below.

Advantages:

- ▷ **Compactness**: smaller footprint, lower material costs, and even transportability, because of the lower weight;
- ▷ **Low Beam-loss**: the highly controlled beam dynamics keeps beam loss to virtually zero along the accelerator, so that a smaller amount of harmful radiation is emitted by the accelerator, dismissing heavy radiation shielding[7];
- ▷ **Modularity**: the cavity internal design is sectioned and the linac can be upgraded by adding more cavities;
- ▷ **Particle Variety**: can be designed to accelerate particles with mass to charge ratio up to 2, such as protons, deuterons, alpha, and stripped carbon ions;
- ▷ **Multi-purpose**: the original design can be adapted to multiple medical and industrial applications of low current and energy beams (e.g., injector in hadron therapy linacs, medical isotope production, material science analysis, semiconductor doping, or polymer modification).

[7] The lower emission of radiation by the accelerator is reasonable, but the complete absence of radiation shielding must yet be confirmed

- ▷ **Low Maintenance**: minimum number of parameters to adjust so that, once tuned, the machine works virtually like a one-button machine and with high reliability.

Limitations:

- ▷ **Low Current**: the smaller aperture, low duty cycle, as well as the narrow energy acceptance are aspects that limit the average output current of the beam;
- ▷ **Conventional Power Requirements**: the demands of the RF power suppliers are as expensive as for conventional linacs and correspond to a considerable portion of the total budget.

1.3 Problem Definition and Approach

By a collaboration agreement, CNPEM and CERN decided to develop a linac to locally supply medical radioisotopes to the PET/MR imaging system of the forthcoming Brazilian BLS-4 laboratory LNMCB. CERN experts suggest a solution based on a compact 750MHz RFQ linac patented by them. The patent covers the principles of beam optics design and the fabrication processes (machining steps and thermal treatments) of the cavity. Indeed, those are cornerstones of an RFQ project, but are very far from being the full solution. This section gives a high level description of the problems and challenges that must be addressed to build a 750 MHz RFQ-based system to produce PET radioisotopes.

The most natural arrangement to design a whole RFQ system is to divide the assignments of the project roughly according to the subsystems of the machine. A complete RFQ system can be divided in:

1. **Ion Gun**: A source of ions must supply the accelerator cavity with low energy ions, usually producing a plasma of the specific ions and guiding them to the first cavity.

2. **RFQ Cavity Design**:

   - **Beam Optics and Cavity Design**: Geometrical specifications of the accelerator must be determined according to the application and the condition of the ions that enters it. Beam optics of the cavity may be determined following the principles of beam optics design patented by CERN and iteratively checking the design with tracking simulations of the particles along the cavity.
   - **Thermal Simulations**: Using a Finite Element Method software, simulations of the cavity heating and cooling dynamics must determine parameters, such as the operating duty cycle of the machine, in order to optimize efficiency, thermal dilation of the cavity and the average output current.

3. **RFQ Cavity Machining**:

- **Cavity Machining and Brazing**: Following the high precision machining steps and thermal treatments determined by CERN, the designed cavity can be machined out of special cooper round ingots.
- **Measurements and Tuning of the Cavity**: The cavity has adjustment devices to resonate the more precise as possible at the designed frequency.

4. **RF Power Source**: Determination of an electromagnetic wave generator to supply the accelerator cavity with RF radiation in enough power and at the right frequency.
5. **Vacuum**: Determination of the solution to evacuate the cavity, such as the desired vacuum pressure, number and type of pumps.
6. **Cooling**: Determination of a cooling solution for the accelerator, usually a water cooler system. Validation of the solution by temperature monitoring.
7. **Beam Diagnostic**: Experimental validation of the working system through output current, emittance and energy measurements.
8. **Control System**: Computers and controllers for all the electronic components.

The subsystems related to the production of PET radioisotopes are:

9. **Target Design**:
   - **Materials and Geometries**: Definition of the materials that will be bombarded by the beam to generate the desired radioisotopes and the geometry of this process.
   - **Yield Simulations**: Simulations of the targets bombardment to foresee the amount of radioisotope activity produced in each irradiation.
10. **Radiation Shielding**: Simulations to determine the radiation shielding of the targets and the accelerator itself.
11. **Radiopharmacy**: Hot laboratories[8] to handle the produced radioactive material and perform all the necessary procedures before injecting them into the subjects.
12. **Facility Floor Plan**: Check how much space each subsystem demands and dispose them in a floor plan.

Most of the points of the project can be resolved using commercial solutions, except for the RFQ cavity design, radiation shielding and floor plan. It is easy to notice that this project demands high specialized human resources from several scientific areas to determine the best solutions and make them work together. Fortunately, CNPEM experts already have considerable experience with cavity machining, RF power sources, vacuum, cooling, beam diagnostics, control system, radiation shielding and floor plan due to Sirius project. The topics related to PET radioisotopes, such as target design and radiopharmacy, can be inspired and improved from cyclotron based

[8] The term "Hot Laboratory" refers to special rooms designed to manipulate radioactive material.

facilities. On the other hand, essential points, such as the ion gun and RFQ design, still need to be studied until we reach a deep enough understanding to find or develop the best solutions to them.

As a first approach to this project, it was decided to start by focusing on essential subsystems to develop a shorter and lower output energy prototype of the accelerator: ion gun, cavity design and machining, RF power source, vacuum, cooling, and beam diagnostic. The two points identified with the highest priority are the ion gun and the RFQ cavity design. This thesis intends to document very preliminary studies made by the author with the objective of learning how to design a high-frequency RFQ cavity.

The design of any linac starts by determining and fixing a list of several key parameters. Some of them depends on the application demands of the machine, such as the accelerated ion species, output energy, and beam current. In the present case, it is important to know which PET radioisotopes are desired, analyse their routes of production and, based on that, decided the best ion species and output energy of the accelerator. This procedure is presented in Chapter 3. The subsequent chapter presents a bibliographic review of 750 MHz RFQ projects.

1.4 Structure of the Thesis

The organization of the present thesis is as follows: after the Introduction and Contextualization provided in the present chapter, Chapter 2 brings theoretical principles and concepts based on textbooks that are useful for the understanding of the researches and discussions presented on the posterior chapters of the thesis. This chapter covers concepts about radioisotope production by activation, RF linacs and RFQs. Chapter 3 describes the ion beam specifications demanded for the production of the desired short half-life PET radioisotopes for the LNMBC. Chapter 4 is dedicated to an overview of, to the best knowledge of the author, all the projects of 750MHz RFQs with published bibliography. At last, the thesis conclusions are presented in Chapter 5.

2 Theoretical Foundations

This chapter contains important concepts, definitions and relations that help the understanding of this thesis. The section about "Radioisotope Production by Activation" provides basis for the understanding of the discussions on chapter "Ion Beam Specification for PET Radioisotopes Production", while the sections about "Radio-frequency Linacs" and "The Radio-frequency Quadrupole" introduce theoretical topics related to the review presented on chapter "The High-frequency RFQ Linacs". For further information and larger explanations, a consultation to the references [8, 24, 25] is recommended.

2.1 Radioisotope Production by Activation

Radioisotopes useful for nuclear medicine can be produced by bombarding nuclei of stable atoms with particles, such as neutrons, protons, and alpha particles to cause nuclear reactions that turn the stable nucleus into an unstable (radioactive) one. The process of transforming stable nuclides into radionuclides is called *Activation*. This section provides some concepts and equations useful for the understanding of this process.

2.1.1 Nuclear Reaction Notation

Most of the nuclear reactions have a target nucleus being bombarded by a projectile particle resulting, after their interaction, in a final nucleus and an ejecting particle. A common way to represent it is

$$\textit{Target Nucleus} + \textit{Projectile} \longrightarrow \textit{Final Nucleus} + \textit{Ejecting Particle}. \tag{2.1}$$

A compact notation to describe a nuclear reaction is the form

$$A(b,c)D \tag{2.2}$$

which is equivalent of a target nucleus A bombarded by the projectile particle b producing an ejecting particle c and a final nucleus D. Typically, light particles are abbreviated, such as p for proton, n for neutron, d for deuteron, α for alpha particle or Helium-4, β for beta particle or electron, γ for gamma photon. The nuclear reaction or sequence of nuclear reactions that transform a stable target material into a desired radionuclide is called *route of production*.

As an example, the production of $^{225}_{89}$Ac is possible when a proton interacts with a $^{226}_{88}$Ra nucleus, ejecting two neutrons. This specific nuclear reaction is denoted by

$$^{226}_{88}\mathrm{Ra}(p,2n)^{225}_{89}\mathrm{Ac}. \tag{2.3}$$

2.1.2 Activity of a Radioactive Sample

Considering a sample containing N radioactive atoms of a certain radionuclide, the decay rate for that sample is given by the differential equation

$$\frac{\mathrm{d}N}{\mathrm{d}t} = -\lambda N \tag{2.4}$$

where λ is the decay constant, which has a characteristic value for each radionuclide. The *half-life* ($T_{1/2}$) is a more usual constant to represent the decay rate of a radionuclide, because it is the time required for the radioactive atoms to decay to 50% of their initial quantity. The half-life and decay constant of a radionuclide are related by

$$T_{1/2} = \frac{\ln 2}{\lambda} \tag{2.5}$$

In equation (2.4), the quantity $\mathrm{d}N/\mathrm{d}t$, the decay rate, is known as *activity* of the sample

$$A = \left|\frac{\mathrm{d}N}{\mathrm{d}t}\right| = \lambda N. \tag{2.6}$$

The activity is the standard measure of "how radioactive" a sample is. In the Système International (SI) the activity unit is the *becquerel* (Bq). One becquerel is defined as the activity of an amount of radioactive material in which one nucleus decays per second. For practical applications, one becquerel is a relatively small unit. For this reason, other units, such as the *curie* (Ci), are also very usual. One curie was originally defined to "express the quantity or mass of *radium emanation* in equilibrium with one gram of Radium (element)"[26], in other words, it was the activity of one gram of ^{226}Ra. However, more accurate measurements changed this value from time to time, until the ^{226}Ra standard was abandoned and fixed in 3.7×10^{10} decays per second. So, the equivalence between these units is

$$1\mathrm{Bq} = 1\mathrm{s}^{-1} = \frac{1}{3.7 \times 10^{10}}\mathrm{Ci}. \tag{2.7}$$

The radioisotope activity divided by the total mass of the sample is called the *specific activity*. Attention must be paid here because textbooks generally use the uppercase A not only for both the activity and the specific activity, but also for mass number. Here, the italic lowercase a was adopted for the specific activity, the italic uppercase A for the activity and the regular uppercase A for the mass number. So, the specific activity can be expressed by

$$a[\mathrm{Bq/g}] = \frac{A[\mathrm{Bq}]}{m[\mathrm{g}]}. \tag{2.8}$$

The highest possible specific activity of a radionuclide is the *carrier-free specific activity* (CFSA). A carrier-free sample is sample purely consisting of a certain radionuclide (meaning that $N/m = N_{av}/\mathrm{A}$). Considering a nuclide with mass number A and half-life time $T_{1/2}$, the carrier-free specific activity is calculated by

$$\mathrm{CFSA}[\mathrm{Bq/g}] = \frac{A[\mathrm{Bq}]}{m[\mathrm{g}]} = \frac{\lambda N}{m} = \lambda\frac{N_{av}}{\mathrm{A}} = \frac{\ln 2}{T_{1/2}} \cdot \frac{N_{av}}{\mathrm{A}}. \tag{2.9}$$

The ^{99m}Tc, for example, has a mass number of A= 99 and half-life time $T_{1/2} = 6$ hours. Therefore, the CFSA of the ^{99m}Tc is

$$\text{CFSA}[^{99m}\text{Tc}] = \frac{0.693}{21.600\text{s}} \cdot \frac{6.023 \times 10^{23}\text{mol}^{-1}}{99\text{g mol}^{-1}} = 1.95 \times 10^{17}\text{Bq/g}. \tag{2.10}$$

2.1.3 Activation Cross-Section

When a sample of a target material is radiated by a particle beam, the amount of activity produced depends on the:

- Intensity of the particle beam (quantified by the flux density ϕ [particles/cm^2/s]);
- Number of target nuclei per volume of the sample (denoted by n [nuclei/cm^3]);
- Probability for a bombarding particle to interact with a target nucleus (determined by the *activation cross-section* σ [1 barn = 1 b = 10^{-24}cm^2].

The activation cross-section for a particular nucleus depends on the bombarding particle, the particular reaction involved and the kinetic energy E of the bombarding particle. Due to the limitations of knowledge about the internal structure of the nucleus, activation cross-sections can only be experimentally measured and, then, are made available in nuclear physics databases. When one knows which radioisotope is desired and its possible routes of production, the plots of $\sigma(E)$ are an essential source of information to guide the choice of bombarding particle species and the kinetic energy of the particle beam.

2.1.4 Activation Rates

To give an initial notion of how the activation process happen, it is interesting to start by considering a bombarding particle beam with flux density ϕ (particles per area per second) passing through a sample with thickness Δx, such as in Figure 20.

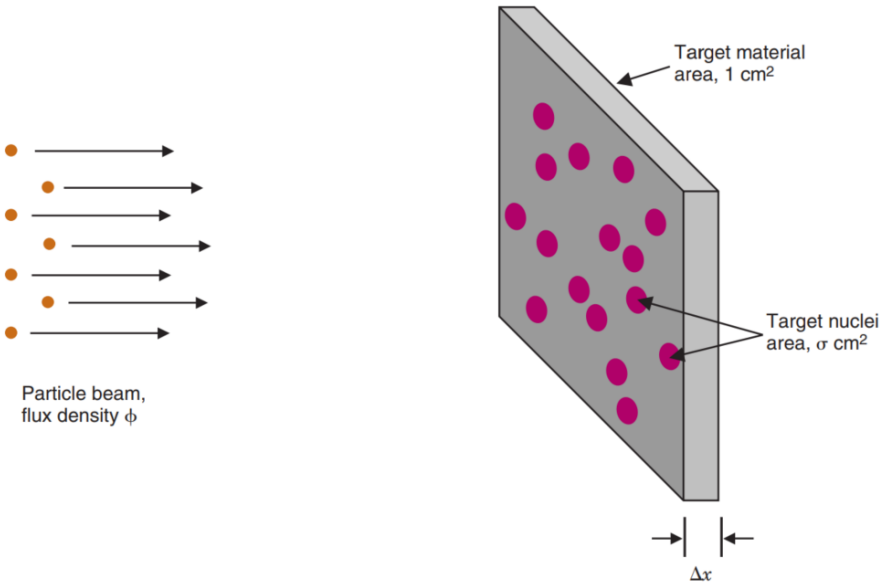

Figure 6 – Bombarding of a thin target material by a particle beam. [8]

Considering that only a single nuclear reaction is occurring, the number R of target nuclei activated and transformed into the final nuclei of this specific nuclear reaction per area per second is equal to the reduction $\Delta\phi$ of the flux density of the beam, which can be expressed by

$$R = -\Delta\phi = n\sigma\phi\Delta x. \tag{2.11}$$

When the geometry of the target is known, it seems easy to just numerically integrate this differential equation along the material and the irradiation time, in order to calculate the total flux reduction and, therefore, the total number of activated nuclei. Then, knowing the half-live of the produced radioisotope, it would be possible to estimate the activity yield of the irradiation. But this is not the case, because this process has much more subtleties. Important points that must be considered for the estimation of the activity yield of the irradiation of a target are:

- The beam particles are decelerated by the target material due to electromagnetic interactions, so that the kinetic energy of the bombarding particles reduces along the material, that is, $E(x)$. This deceleration, generally referred as *stopping power* ($\mathrm{d}E/\mathrm{d}x$), must be experimentally measured beforehand, because of the energy-dependence of the activation cross-section $\sigma(E)$. In other words, the calculation must consider a composition of two experimentally measured functions $\sigma(E(x))$;
- The number of particles of the beam reduces not only because of the desired nuclear reaction but also because of any other possible nuclear reaction, known as parasitic reactions. It must be considered because if a considerable portion of the bombarding particles is activating other nuclear reactions beyond the desired one, the production yield can be drastically reduced.

These points increase the complexity of the activation process so that the calculation of production yields can only be satisfactorily estimated with analytical and computational calculations based on databases of experimental measurements.

2.2 Radio-frequency Linacs

The term *linear accelerator* (and its abbreviation *linac*) commonly refers to an accelerator in which charged particles are accelerated by time-dependent electromagnetic fields through a linear path. In a radio-frequency linac (*RF linac*), a beam of charged particles is accelerated by harmonic time dependent RF electromagnetic fields. This section starts presenting common types of RF linac structures, then reviews important relations about relativistic particles traveling in electromagnetic fields and the constrains of resonant cavities on Maxwell's equations, which are essential concepts to understand how these machines are capable of accelerating charged particles.

2.2.1 Common Linac Structures

The first RF linear accelerator was proposed and experimented by Wideröe in 1928 at Aachen, Germany. [27] Wideröe's linac concept was to apply time-alternating voltage

to drift tubes placed in a linear sequence, as presented in Figure 7. This accelerator was capable of accelerating a beam of singly charged potassium ions to a final energy of 50 keV using an RF voltage of 25 kV, *i. e.*, the ions obtained twice the energy from a single application of the voltage.

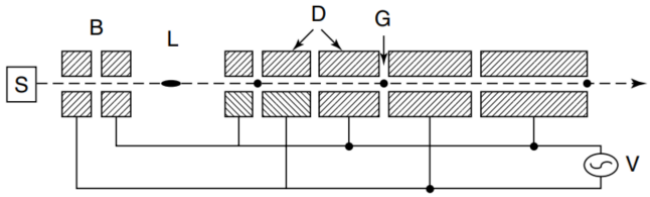

Figure 7 – Concept of the Wideröe's drift-tube linac. The drift tubes (D) were made out of a conducting material and connected to an alternating voltage source (V). The opposite voltages applied to sequential drift tubes generate electric fields in the gaps (G) between them. After passing through a bunching (B) and velocity modulation in a suitable drift space (L), the particles coming from the continuous ion beam source (S) gain kinetic energy every time they cross a gap between the drift tubes. The particles must arrive every gap at the right time to be accelerated, for this reason the length of the drift tubes increases with increasing particle velocity. [24]

A rather common and modern way to accelerate charged particles is to excite a RF standing wave in a multicell or coupled-cavity array. One type of structure is the Alvarez Drift Tube Linac (Alvarez DTL), where drift-tubes are linearly disposed within a conducting cylindrical cavity, as show in Figure 8. It is used to accelerate already bunched beams of protons and other ions in a velocity range from around 0.04 to 0.4 times the speed of light. Above the velocity of 0.4 times the speed of light, coupled-cavity structures are used, like the side-coupled linac (SCL) presented in Figure 9. High-velocity particles can also be accelerated by superconducting cavities, which are highly energy effective and usually made out of Niobium alloys with the geometry presented in Figure 10.

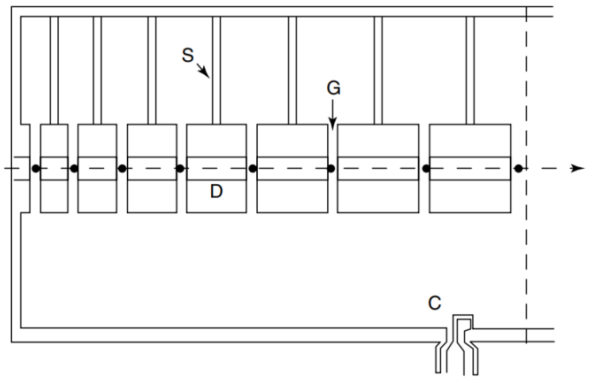

Figure 8 – Concept of Alvarez DTL. Excited by an external RF current flowing on a coaxial line into the loop coupler (C), a resonating mode inside the cavity creates an alternating uniform electric field in the gaps (G) and no field inside the drift tubes (D), that are supported by stems (S). Just like in the Wideröe accelerator, the drift-tubes have increasing lengths, so that the particles avoid deceleration when the field is reversed. [24]

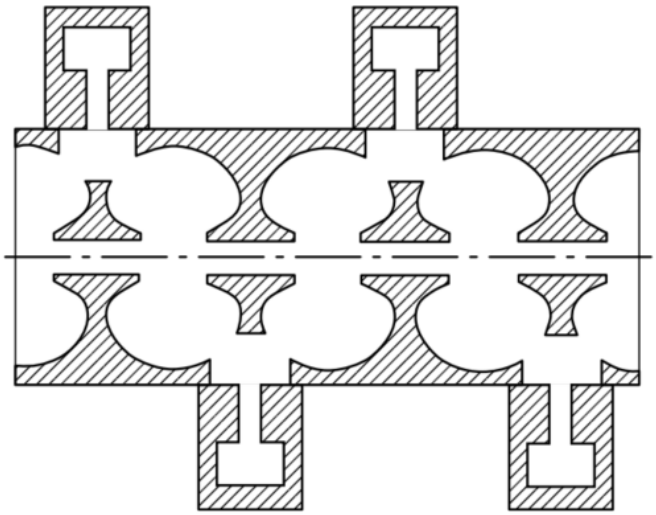

Figure 9 – Example of a coupled-cavity structure, the side-coupled linac. The cavities on the beam axis are responsible for accelerating the particles, while the cavities on the side are unexcited and provide stabilization of the fields against perturbations due to machining errors and beam loading. [24]

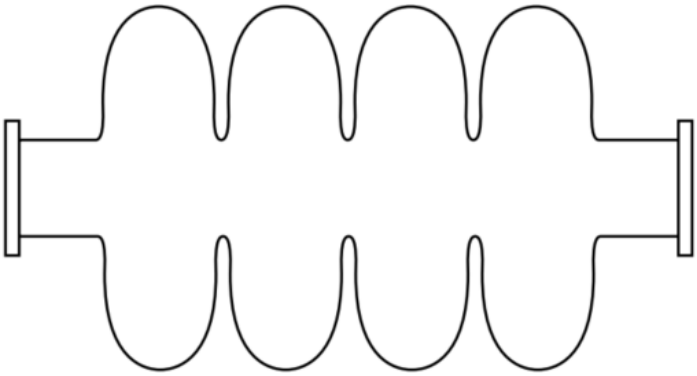

Figure 10 – Cross section of a superconducting cavity. The elliptical shape is universally accepted for a superconducting cavity shape because of its low ratio of peak surface field to average axial field and practical advantages for drainage of fluids during chemical processing. [24]

As these structures are not able to provided transverse-focusing for the beam, magnetic-quadrupole lenses must be mounted within the DTL and between the structures of coupled-cavity linacs. Though, there exists a very clever resonating cavity structure that is capable of both accelerating and focusing ions in a very-low-velocity range from about 0.01 to 0.06 times the speed of light, the Radio Frequency Quadrupole (RFQ). This structure was very innovative when is was firstly presented because it significantly improves the quality of beam extraction from ion sources and injection into higher energy linacs. More details about RFQ structure and its working principles are given on Section 2.3. Figure 11 shows how the velocity of a proton increases in function of its kinetic energy (obeying the relativistic relations presented in the following Subsection 2.2.2) and summarizes the typical range of velocities and energies suited for the linac structures introduced in this section.

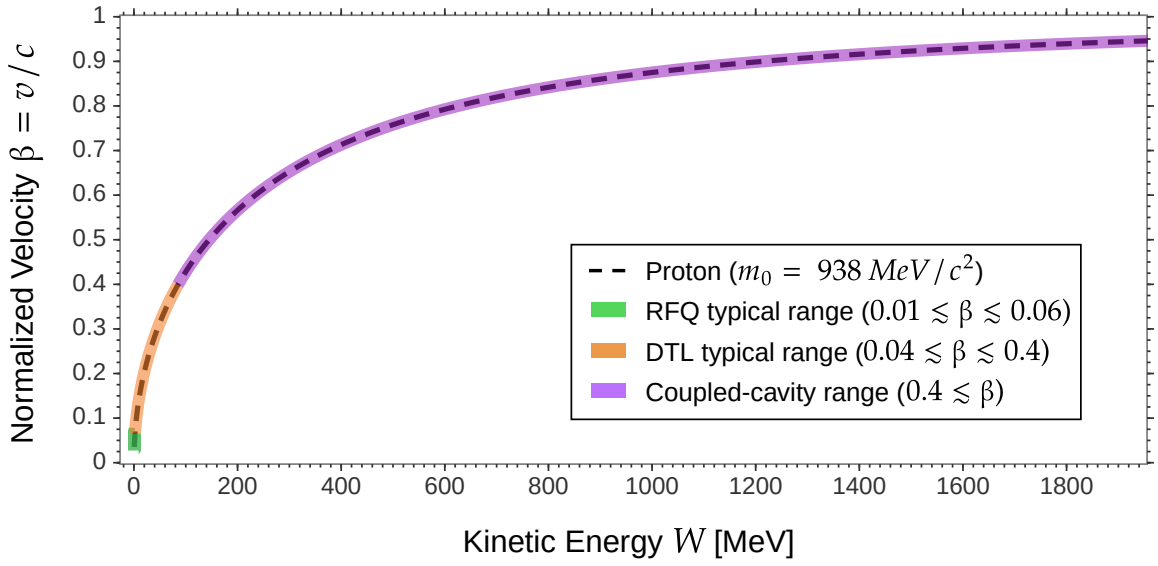

Figure 11 – Normalized velocity β of a proton in function of its kinetic energy W. The colors over the curve highlight the range of velocities in which the most common RF linac structures RFQ, DTL and coupled-cavities are suited.

2.2.2 Relativistic Particles in Electromagnetic Fields

Considering a particle with rest mass m_0, carrying a charge q, and traveling at a velocity $\mathbf{v}$, it is usual to normalize its velocity according to the speed of light c:

$$\boldsymbol{\beta} = \mathbf{v}/c \tag{2.12}$$

and to define the relativistic mass factor

$$\gamma = 1/\sqrt{1-\beta^2}. \tag{2.13}$$

In function of these factors, the relativistic momentum is given by

$$\mathbf{p} = \boldsymbol{\beta}\gamma m_0 c. \tag{2.14}$$

and the kinetic energy is

$$W = (\gamma - 1)m_0c^2, \tag{2.15}$$

Traveling through an electromagnetic field, the momentum $\mathbf{p}$ changes according to the Lorentz force:

$$\frac{\mathrm{d}\mathbf{p}}{\mathrm{d}t} = \mathbf{F} = q(\boldsymbol{E} + \mathbf{v} \times \boldsymbol{B}). \tag{2.16}$$

In particle accelerators, both electric and magnetic components of the Lorentz force provide steering and focusing capabilities, but only the electric field can change the kinetic energy of the particles. A particle traveling a short distance $\mathrm{d}z$ along the z-axis through an axis-parallel electric field E_z has its kinetic energy changed by

$$dW = qE_z dz. \tag{2.17}$$

2.2.3 Maxwell's Equations and EM Fields in Resonant Cavities

Classical electrodynamics are described by Maxwell's equations, which have the following differential representation in the most general case:

$$\boldsymbol{\nabla} \times \boldsymbol{H}(\boldsymbol{r},t) = \frac{\partial}{\partial t}\boldsymbol{D}(\boldsymbol{r},t) + \boldsymbol{J}(\boldsymbol{r},t), \tag{2.18}$$

$$-\boldsymbol{\nabla} \times \boldsymbol{E}(\boldsymbol{r},t) = \frac{\partial}{\partial t}\boldsymbol{B}(\boldsymbol{r},t), \tag{2.19}$$

$$\boldsymbol{\nabla} \cdot \boldsymbol{D}(\boldsymbol{r},t) = \rho(\boldsymbol{r},t), \tag{2.20}$$

$$\boldsymbol{\nabla} \cdot \boldsymbol{B}(\boldsymbol{r},t) = 0, \tag{2.21}$$

where $\boldsymbol{H}$ and $\boldsymbol{E}$ denote the magnetic and electric field strengths, $\boldsymbol{B}$ and $\boldsymbol{D}$ the corresponding flux densities, ρ the electric charge density and $\boldsymbol{J}$ the electric current density.

In the absence of free charges and assuming harmonic time dependence $e^{j\omega t}$, it is possible to combine the equations and get the well-known Helmholtz equations of the electric and magnetic fields:

$$(\boldsymbol{\nabla}^2 + k^2)\boldsymbol{E}(\boldsymbol{r},\omega) = 0, \tag{2.22}$$

$$(\boldsymbol{\nabla}^2 + k^2)\boldsymbol{H}(\boldsymbol{r},\omega) = 0. \tag{2.23}$$

If the frequency is low and the wavelength becomes larger than compared to the geometry of interest, the fields can be described by the so-called quasi-static approximation. In this regime, the electric field is curl-free and can be written as the gradient of an electrostatic potential Φ:

$$\boldsymbol{E}(\boldsymbol{r},\omega) = -\boldsymbol{\nabla}\Phi(\boldsymbol{r})\sin(\omega t + \phi), \tag{2.24}$$

where Φ satisfies the Laplace equation in absence of charges:

$$\boldsymbol{\nabla}\Phi(\boldsymbol{r}) = 0 \tag{2.25}$$

and ϕ is the phase of the electric field oscillation.

Inside an RF cavity, the waves are inside a volume bounded by conducting walls, such that standing waves are established. Considering the walls of very high conductance, called perfect electric conductor (PEC), the fields are subjected to the following boundary conditions:

$$\boldsymbol{n} \times \boldsymbol{E} = 0 \qquad \text{and} \qquad \boldsymbol{n} \cdot \boldsymbol{H} = 0 \qquad \text{on} \qquad \partial \boldsymbol{V}_{PEC}, \tag{2.26}$$

with $\boldsymbol{n}$ indicating the boundary normal.

The combination of the equations (2.22) and (2.23) with the boundaries (2.26) leads to an eigenvalue problem. The fields that fulfill the eigenvalue problem are commonly denoted as the eigenmodes of the cavity, which are mutually orthogonal.

The discrete oscillation frequencies are the eigenfrequencies $\omega_n = k_n c$, derived from the eigenvalues k_n^2. The eigenmodes in a bounded cylindrical volumes can be either Transverse Electric (TE) or Transverse Magnetic (TM). In TE modes the electric field is perpendicular to the direction of propagation while in TM modes the magnetic field is perpendicular to the direction of propagation. They are denoted as TE_{nml} and TM_{nml}, respectively, where the index n, m, l refer to the azimuthal, radial and longitudinal components. Examples of TE modes in empty cavities are shown Figure 12.

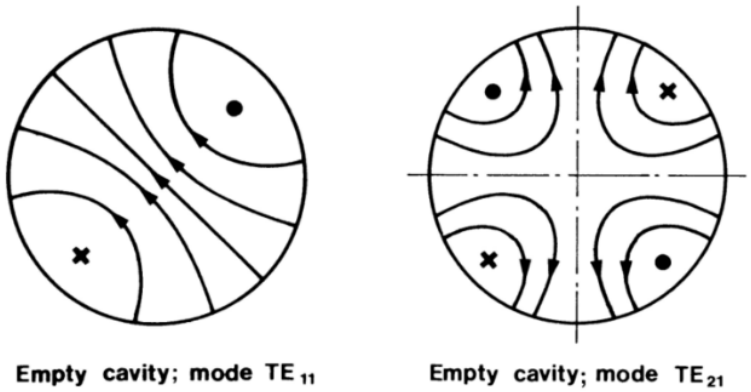

Figure 12 – Dipole mode TE_{110} and quadrupole mode TE_{210} in a cylindrical empty cavity. The electric fields are in the transverse plane (paper plane) while the magnetic field are in the longitudinal direction (perpendicular to the paper plane). [25]

2.3 The Radio-frequency Quadrupole

The radio-frequency quadrupole is a special type of RF resonant cavity linac developed for very-low-velocity range invented by Kapchinskij and Teplyakov at the USSR Institute for High Energy Physics in Protvino in the late 1960's. [28, 29] The cavity of an RFQ is subdivided into four quadrants separated by vanes and interconnected in the center, as shown in Figure 13. Due to the four vanes, the cavity forces the RF fields to resonate in the TE_{210}, which is a mode able to focus the beam in the transverse plane. Kapchinskij and Teplyakov proposed a spatial sinusoidal-like modulation to the tip of the vanes, which introduces a longitudinal electric field component able to accelerate the ions. The simultaneously of acceleration, focusing and bunching minimises the beam loss and generate beams with excellent output quality. For this reason, this invention is considered a major innovation in the field of linacs and, nowadays, it is usually the first accelerating structure of hadron accelerators.

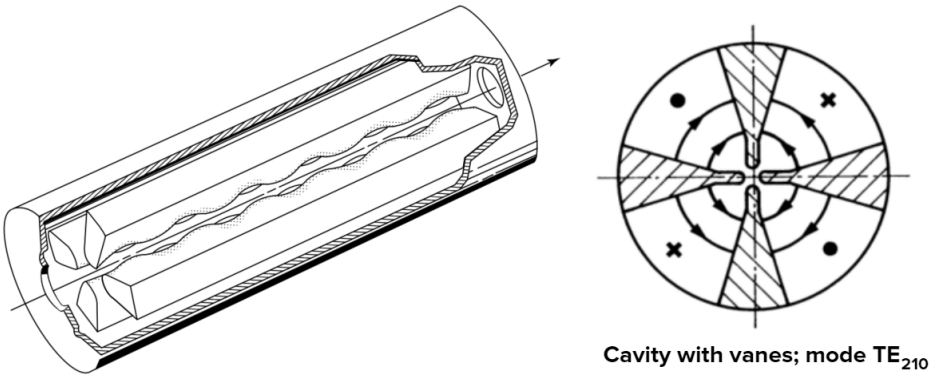

Figure 13 – Four-vane RFQ accelerator section representation. The RF radiation excites the four electrodes within the cavity to focus the beam using the quadrupole mode TE_{210}. The electrode tips have a sinusoidal shape modulation which produces longitudinal electric fields that accelerate and bunch the low-velocity ions. [24, 25]

As seen in Figure 14, the modulation of the vanes that face each other is the same, while between the vanes that are orthogonal, the modulations are out of phase so that the minimum modulation in one vane coincides with the maximum modulation of the other vane. The oscillations on the tips of the RFQ defines a sequence of longitudinal unit cells. As the magnitude of the fields depends on the distance between the vanes, the design of an RFQ is given by the definition of three parameters for each unit cell along the cavity:

- the *Aperture* a, which is the minimum distance from the tip to the axis;
- the *Modulation Factor* m, which is the ratio between the maximum and minimum distance from the axis;
- and the *Synchronous Phase* ϕ_s, which is controlled by controlling the center-to-center spacing of the unit cells, achieving acceleration.

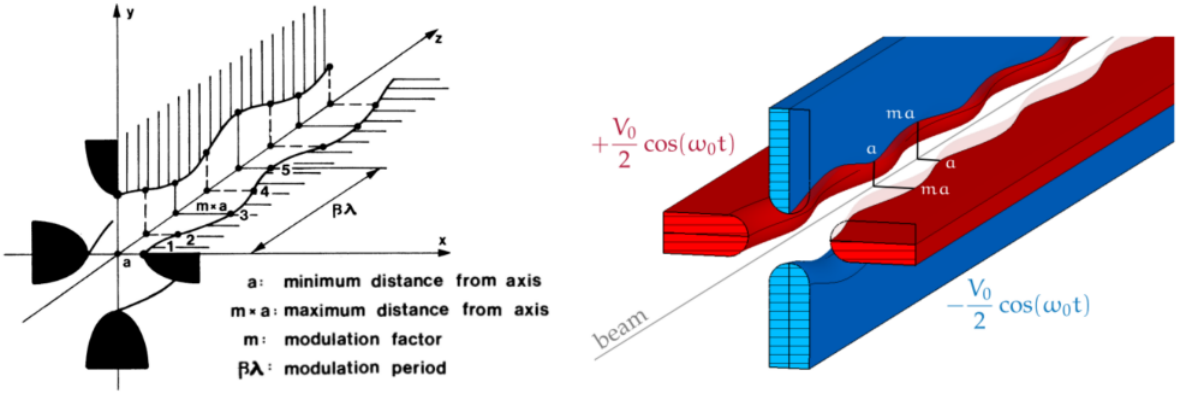

Figure 14 – Modulation of the RFQ unit cells to control the accelerating longitudinal fields and the transverse focusing fields. [25, 30]

In the following subsections, some equations are presented to help the understanding of how these parameters effect the fields among the tips of the RFQ and thus

the motion of the ions, called *beam dynamics*, both in longitudinal and transverse directions along the cavity. The transverse beam dynamics is discussed more qualitatively, because it would demand the presentation of other concepts that are beyond of what the time allowed the author to learn. Nevertheless, the longitudinal dynamics was still presented while certain depth.

2.3.1 Potential Function in an RFQ Cell

The general solution for a idealized periodic RFQ structure can be expressed as an infinite Fourier-Bessel series:

$$\Phi(r,\theta,z) = \frac{V_0}{2}\left[\sum_{\nu=0}^{\infty} A_{0,\nu} r^{2\nu}\cos(2\nu\theta) + \sum_{\mu=1}^{\infty}\sum_{\nu=0}^{\infty} A_{\mu,\nu} I_{2\nu}(\mu k r)\cos(2\nu\theta)\cos(\mu k r)\right] \quad (2.27)$$

where, V_0 is the potential between orthogonal vanes (Figure 14), μ and ν are respectively the longitudinal and azimuthal indices, I_n denotes the modified Bessel function of the first kind and order n, $k = \pi/L = 2\pi/\beta\lambda$ identifies the spatial wavenumber of the cell, and $A_{\mu,\nu}$ are the coefficients of the series expansion.

To simplify the analysis, let us consider only the two first terms of each infinite series:

$$\Phi(r,\theta,z) = \frac{V_0}{2}\left[A_{0,1} r^2\cos(2\theta) + A_{1,0} I_0(kr)\cos(kz)\right], \quad (2.28)$$

where the first term is recognized as the potential of an electric quadrupole, while the second term gives the accelerating field.

Imposing the condition that $\Phi(r,\theta,z)$ is constant along a vane (check Figure 14):

$$\Phi(a,0,0) = \Phi\left(ma, 0, \frac{\beta\lambda}{2}\right) = \frac{V_0}{2}, \quad (2.29)$$

the coefficients $A_{1,0}$ and $A_{1,0}$ result in

$$\text{Acceleration Parameter:} \qquad A_{1,0} = \frac{m^2-1}{m^2 I_0(ka) + I_0(mka)} \quad (2.30)$$

$$\text{Focusing Parameter:} \qquad A_{0,1} = \frac{1}{a^2}\cdot\frac{I_0(ka)+I_0(mka)}{m^2 I_0(ka)+I_0(mka)} = \frac{\chi}{a^2}. \quad (2.31)$$

The field components, in cylindrical coordinates, derived from the potential 2.28 are

$$E_r = -\frac{\partial\Phi}{\partial r} = -\frac{V_0}{2}\left[2A_{0,1} r\cos(2\theta) + kA_{1,0} I_1(kr)\cos(kz)\right], \quad (2.32)$$

$$E_\theta = -\frac{1}{r}\frac{\partial\Phi}{\partial\theta} = V_0 A_{0,1} r\sin(2\theta), \quad (2.33)$$

$$E_z = -\frac{\partial\Phi}{\partial z} = \frac{V_0}{2} k A_{1,0} I_0(kr)\sin(kz). \quad (2.34)$$

Figure 15 helps the visualization of the electric field given by the equation above by showing sections of the RFQ near its axis and filling the empty spaces with

a color gradient representing the potential and arrows representing the electric field. The top figures depict the transverse electric field at the beginning, center and end of the cell. Looking at these figures we can check that the transverse electric field has horizontal components pointing inwards the center of the cross-section and vertical components pointing outwards. These components, which are usually much stronger than the longitudinal component, are responsible for giving a horizontal focusing and a vertical defocusing to the ions along this cell. The opposite occurs along the next cell, i. e., the beam receives a horizontal defocusing and a vertical focusing. This alternating focusing and defocusing effects cause the ions of beam to gradually concentrate very near the axis of the accelerator. This concentration of ions is not easy to describe due to the so-called *space charge*, which is nothing more than the Coulomb repulsion between the charged particles of the beam, that are all equally charged. This repulsion effect is particularly strong when the ions have velocities much smaller than the speed of light (non-relativistic particles), and becomes weaker when the particles reach relativistic velocities. The bottom figure shows the longitudinal component of the field in the horizontal and vertical planes, which is the electric field component that accelerates the particle in the longitudinal direction. The longitudinal motion of the ions are presented in the next subsection.

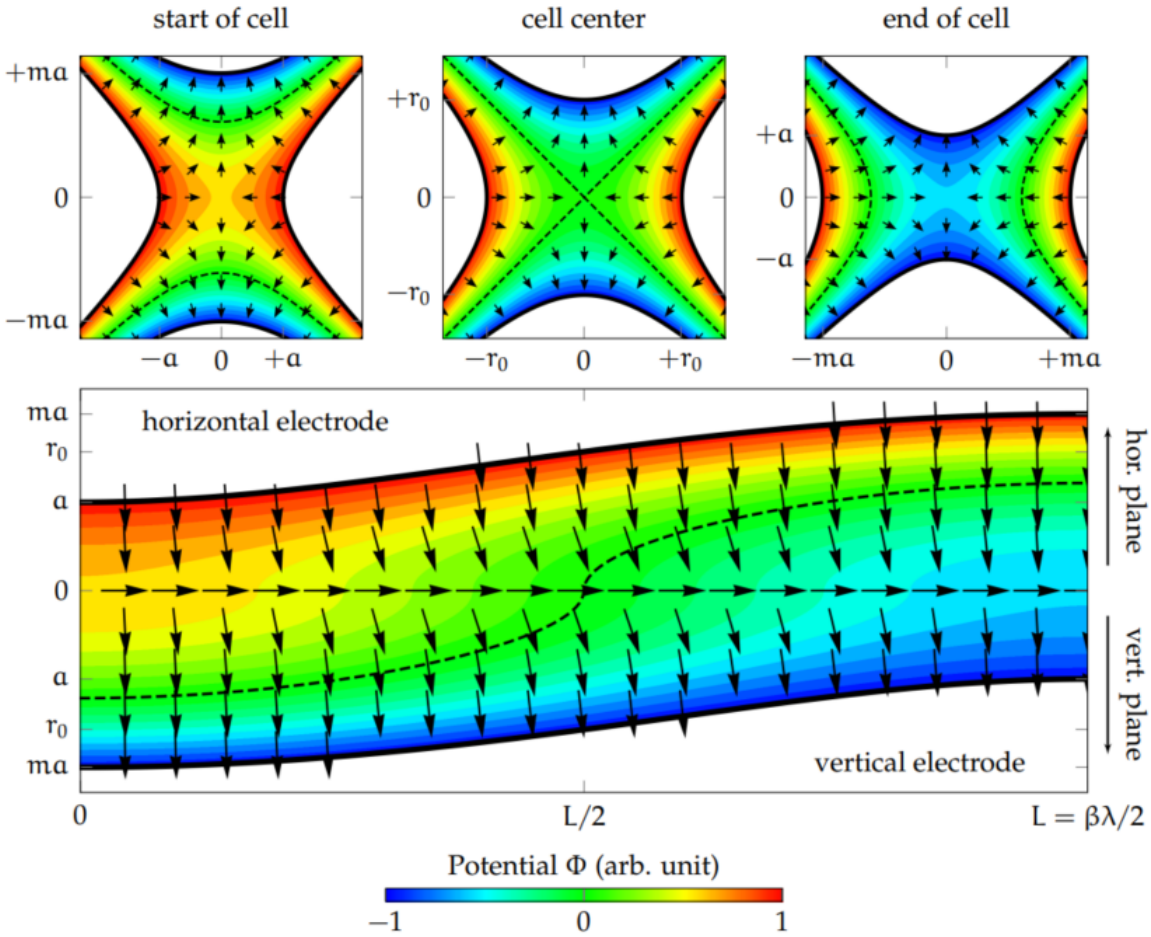

Figure 15 – Visualization of the two-term potential function in a RFQ cell. The top diagrams depict the transverse electric fields at the beginning, center, and end of an RFQ cell, while the bottom diagram shows the fields in horizontal and vertical plane. Dashed lines are equipotential surfaces. [30]

2.3.2 Longitudinal Beam Dynamics

The longitudinal beam dynamics of an RFQ is very similar to other linear accelerators. The motion of the particles along this direction is usually described by taking for reference the *synchronous particle*. The synchronous particle is the one that crosses a unit cell with the specific kinetic energy W_s and the specific position relative to the EM field (denoted by the phase ϕ_s relative to the field phase) so that the particle gains the right amount of kinetic energy to keep its phase stable (constant) while traveling through that cell of the accelerator.

We start considering a test particle of charge q, velocity β, kinetic energy W and phase ϕ_s with respect to the EM field phase. This particle sees the longitudinal electric field given by equations (2.24), (2.34) and the constrain $\omega t = kz$ between the radiation frequency and the RFQ cell length:

$$E_z(r,\theta,z) = -\frac{\partial \Phi}{\partial z}\sin(\omega t + \phi) = \frac{V_0}{2}kA_{1,0}I_0(kr)\sin(kz)\sin(kz+\phi). \tag{2.35}$$

The kinetic energy gain of that charge along a cell of the RFQ is given by the integration of equation (2.17). We can use the relations $L = \beta\lambda/2 = \pi/k$ and $\omega t = 2\pi z/(\beta\lambda) = kz$ to perform the integration, which results:

$$\begin{aligned}
\Delta W &= \int_0^L qE_z(r,\theta,z)dz \\
&= q\frac{V_0}{2}kA_{1,0}I_0(kr)\int_0^{\beta\lambda/2}\sin(kz)\sin(kz+\phi)dz \\
&= q\frac{V_0}{2}kA_{1,0}I_0(kr)\left(\frac{\pi}{2}\frac{\cos(\phi)}{k}\right) \\
&= \frac{\pi}{4}qV_0A_{1,0}I_0(kr)\cos(\phi).
\end{aligned} \tag{2.36}$$

The energy gain of a particle in a cell is independent of the cell length, but dependent on the intervane voltage V_0 and the phase of the particle relative to the field. We know that the synchronous particle is the one that keeps phase and energy stability along the acceleration cell. It is canonical to evaluate the longitudinal stability of our test particle relative to the synchronous particle using the following variables:

$$\Delta\phi = \phi - \phi_s \tag{2.37}$$

$$\Delta W = W - W_s \tag{2.38}$$

which indicate the phase and energy differences between the test particle and the synchronous one.

Assuming an adiabaticity approximation ($\beta = constant$), i.e. a very small acceleration, and following some algebra present in the reference [24], it is possible to obtain a very interesting curve on the (ΔW, ϕ) phase space called *separatrix*. The separatrix defines the area within which the test particles have stable trajectories and stay near the synchronous particle. This curve represents the limits of a potential well with a minimum at the synchronous phase point, as can be seen in Figure 16. The points on the separatrix satisfy the equation

$$\frac{Aw^2}{2} + B(\sin\phi - \phi\cos\phi_s) = -B(\sin\phi_s - \phi_s\cos\phi_s) \tag{2.39}$$

where w, A and B are

$$w \equiv \frac{\Delta W}{mc^2},\ A \equiv \frac{2\pi}{\beta_s^3 \gamma_s^3 \lambda} \text{ and } B \equiv \frac{qE_0T}{mc^2}. \tag{2.40}$$

The separatrix is also called *fish*, and the stable area within it is called *bucket*. This curve is important for the design of an accelerator because the size of the stable area is determined by the synchronous phase, which is a parameter that must be chosen for each cell along an RFQ. The synchronous phase usually starts being equal to $-90°$, where no acceleration is accomplished but the acceptance of the stable area is the highest, and rises to around $-30°$, when the stable area becomes smaller but the particles receive more acceleration per cell.

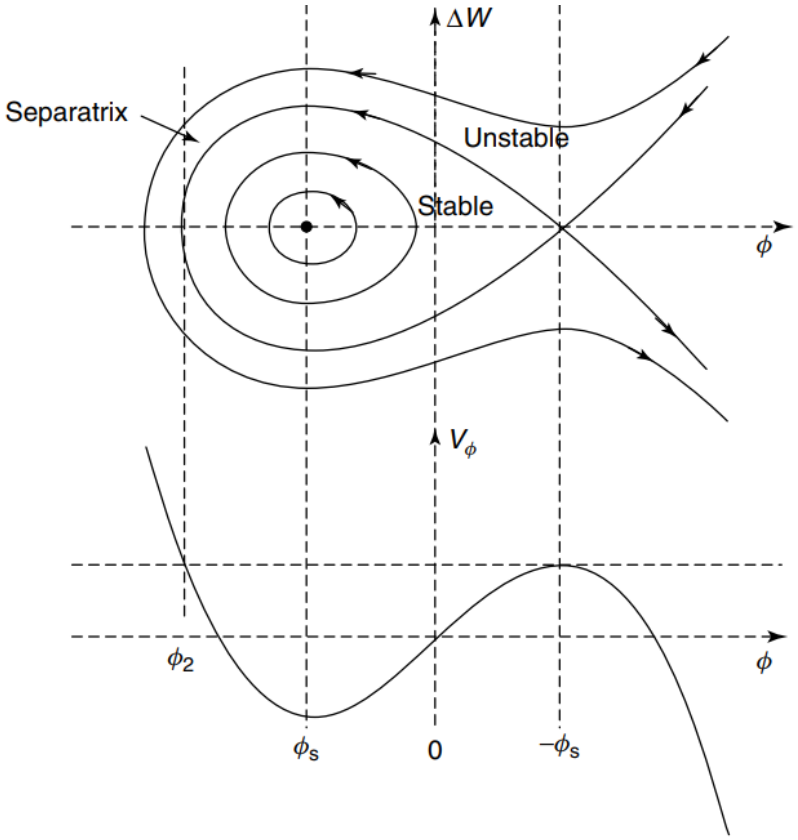

Figure 16 – The synchronous phase ϕ_s is shown as a negative number where the field is rising in time. The top plot shows the longitudinal phase space, including the separatrix, that limits the stable area of the phase space. We can see that the synchronous phase is not the only fixed point. The phase $\phi = -\phi_s$ is also a fixed point, but an unstable one. [24]

3 Ion Beam Specification for PET Radioisotopes Production

When designing a linear accelerator, it is essential to know the demands of its application because they define the aimed specifications of the machine. In our case, the linear accelerator must be designed to produce an ion beam with enough current, energy and size to produce PET radioisotopes in sufficient amounts to be injected into small animals. According to it, at least four basic parameters have to be determined:

- What ion must the linac accelerate?
- The ions must leave the accelerator with how much kinetic energy?
- How much must the beam current be?
- What size must the beam have?

The initial focus of the study was to answer the two first questions above, because the beam current and size usually are parameters limited by the linear accelerator. This study was carried out based on the nuclear reaction database documented by IAEA [31] and following the procedures presented below roughly in that order:

1. Research and listing of the PET radioisotopes that accelerators typically produce;
2. Determination of the desired PET radioisotopes for the LNMCB;
3. Analysis of the typical routes of production of the selected radioisotopes and their respective activation cross-sections;
4. Determination of the bombarding ion to produce the selected radioisotopes;
5. Determination of an output energy range for the accelerator according to the activation cross-sections.

The radioisotopes listed on Table 1 are traditional positron (β^+) emitters used in PET imaging systems that can be produced by accelerators, especially cyclotrons facilities [32].

Table 1 – Some typical nuclear reactions for the production of diagnostic PET radioisotopes made available in an IAEA nuclear database. [33]

PET radionuclide	Half-life	Decay (%)	Reaction product	Half-life	Decay (%)	Production reaction
^{11}C	1221.8 sec	99.7669 β^+	^{11}C	1221.8 sec	99.7669 β^+	$^{14}N(p,\alpha)^{11}C$
^{13}N	9.965 min	99.8036 β^+	^{13}N	9.965 min	99.8036 β^+	$^{16}O(p,\alpha)^{13}N$
^{15}O	122.24 sec	99.9003 β^+	^{15}O	122.24 sec	99.9003 β^+	$^{15}N(p,n)^{15}O$ $^{14}N(d,n)^{15}O$
^{18}F	109.77 min	96.73 β^+	^{18}F	109.77 min	96.73 β^+	$^{18}O(p,n)^{18}F$ $^{nat}Ne(d,x)^{18}F$
^{68}Ga	67.71 min	88.91 β^+	^{68}Ge	270.95 d	100 EC	$^{69}Ga(p,2n)^{68}Ge$ $^{nat}Ga(p,xn)^{68}Ge$
^{82}Rb	1.2575 min	95.43 β^+	^{82}Sr	25.35 d	100 EC	$^{85}Rb(p,4n)^{82}Sr$ $^{nat}Rb(p,xn)^{82}Sr$

At the moment, the desired PET radioisotopes for the LNMCB are ^{11}C, ^{13}N, ^{15}O e ^{18}F [34]. Carbon, Nitrogen and Oxygen are very important elements because they constitute organic molecules of the living organisms and can be used to label a variety of useful pharmaceutical compounds [35]. The short half-life of their isotopes ($^{11}C \approx 20.4$ minutes; $^{13}N \approx 10$ minutes; $^{15}O \approx 2$ minutes) demands a local production and fast manipulation to guarantee enough amount of activity during the PET exam. Fortunately, that is not a problem in our case because the accelerator shall be installed in the same building as the PET system. The isotope of Fluorine was chosen because it is the most popular and successful PET radioisotope. The popularity of this isotope is due to the low energy demanded to produce it and the versatility of the pharmaceutical [^{18}F]FDG. In our case, it will be injected in small animals, but this radiopharmaceutical is widely used to diagnose a variety of diseases in humans, such as Alzheimer's disease, infections, many types of cancer, as well as to evaluate treatment outcomes [36, 37]. Recently, even lung lesions caused by COVID-19 were characterized by [^{18}F]FDG using a PET/CT [38].

To produce the four desired radioisotopes, we can already conclude by the reactions presented on Table 1 that the bombarding particle must be a proton. In the next sections, the activation cross-section of the reactions to produce these PET isotopes are presented in order to evaluated the energy range in which they are produced.

3.1 Carbon-11

^{11}C is obtained from the collision of protons on the ordinary isotope of Nitrogen ^{14}N in the form of N_2 mixed with trace amounts of oxygen or hydrogen. The nuclear reaction $^{14}N(p,\alpha)^{11}C$ has a threshold energy of around 4 MeV and a optimal energy production around 7 to 8 MeV, with a cross-section peak of around 250 mb. It can be applied as [^{11}C]CO_2 or [^{11}C]CH_4, but other applications of ^{11}C can be found on references [39, 40].

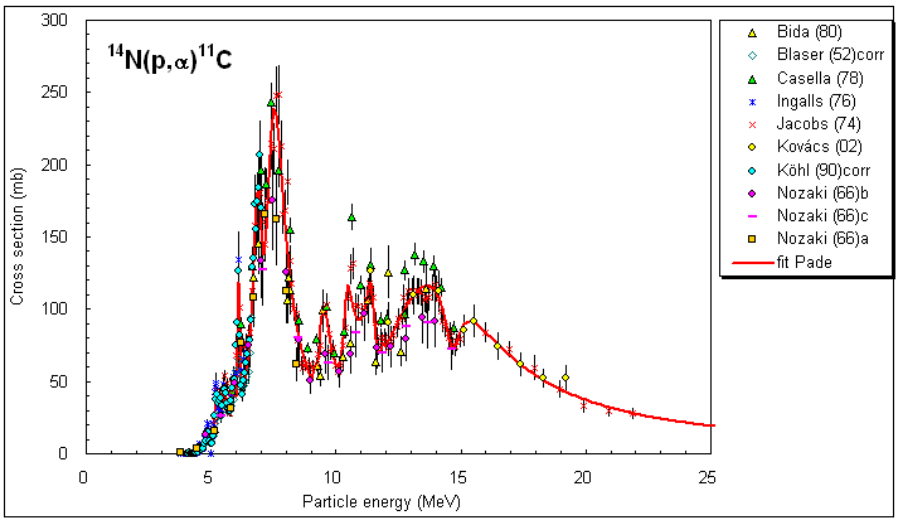

Figure 17 – Cross section for the ^{14}N(p,α)^{11}C nuclear reaction. [31]

3.2 Nitrogen-13

From the collision of protons on the ordinary isotope of Oxygen ^{16}O, ^{13}N can be obtained. The nuclear reaction ^{16}O(p,α)^{13}N has a threshold energy of around 6 MeV and a optimal energy production from 7.5 to 8.5 MeV, with a narrow cross-section peak of 180 mb. This isotope can be applied specially in the form of ammonia [^{13}N]NH_3 [41].

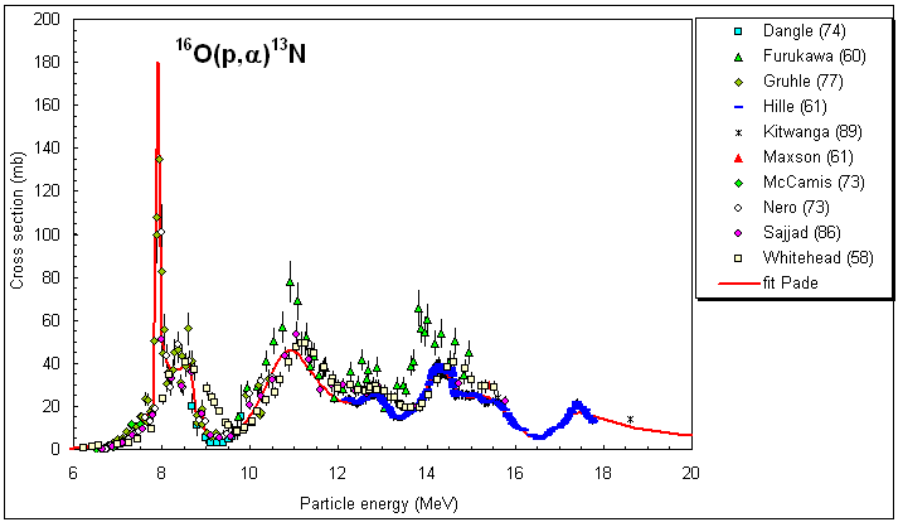

Figure 18 – Cross section for the ^{16}O(p,α)^{13}N nuclear reaction. [31]

3.3 Oxygen-15

To produce ^{15}O with accelerated protons, the option is to bombard the stable but rare isotope of Nitrogen ^{15}N. The nuclear reaction ^{15}N(p,n)^{15}O has a threshold at 4 MeV and a optimal production within 5.5 - 7.5 MeV, with around 150 mb of cross-section. The ^{15}O is commonly applied as simple components like [^{15}O]CO_2 and [^{15}O]H_2O,

because its extremely short half-live makes very difficult the synthesis of other labeled components [5]. The development of ultra-fast synthesis is a way to overcome it, such as reported in [42].

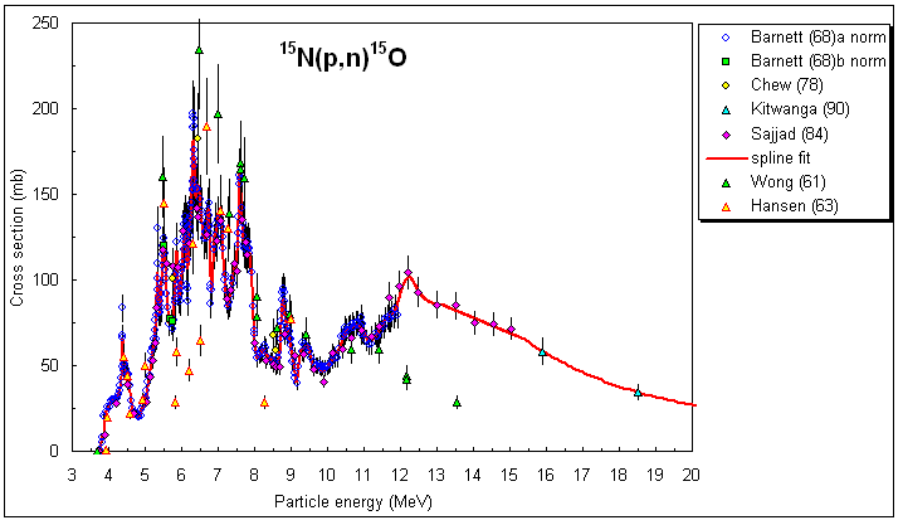

Figure 19 – Cross section for the ^{15}N(p,n)^{15}O nuclear reaction. [31]

3.4 Fluorine-18

The dominant PET isotope ^{18}F can be generated by the proton bombardment of water enriched with the stable isotope of Oxygen ^{18}O. The reaction ^{18}O(p,n)^{18}F has a threshold around 2.5 MeV and a high activation cross-section between 5 and 6 MeV, with a peak of 510 mb. It is possible to see that the cross-section of the reaction has considerable high values along a wide range of energy, meaning that the production of this isotope is very efficient for various energies.

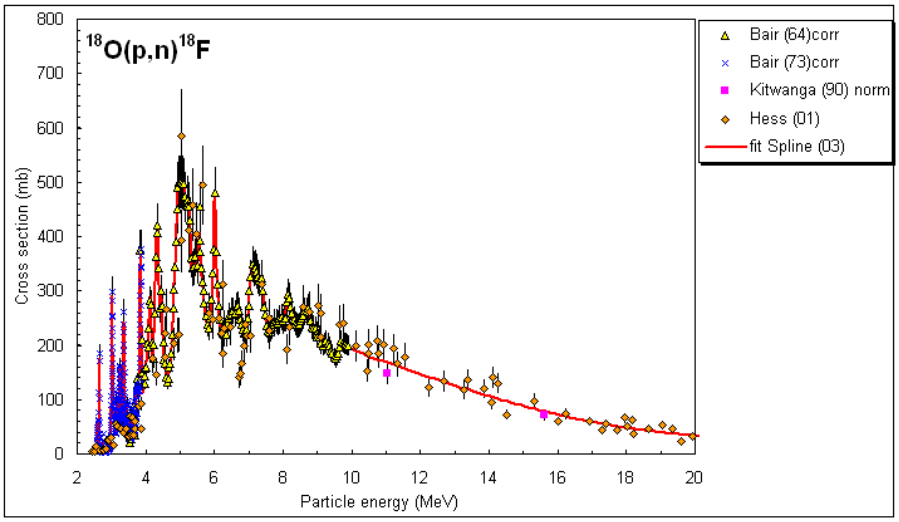

Figure 20 – Cross section for the ^{18}O(p,n)^{18}F nuclear reaction. [31]

3.5 Conclusion

After the analysis of the activation cross-sections of the chosen nuclear reactions, it is possible to reach certain conclusions about the ion beam proprieties suited to produce PET isotopes for the LNMCB. Table 2 summarizes the information gathered from the cross-sections.

Table 2 – Summary of energy demands for selected PET radioisotopes production using protons.

PET radionuclide	**Production reaction**	**Threshold Energy** [MeV]	**Optimal Energy Range** [MeV]	**Cross-section Peak** [mb]
^{11}C	$^{14}N(p,\alpha)^{11}C$	4	7-8	250
^{13}N	$^{16}O(p,\alpha)^{13}N$	6	7.5-8.5	180
^{15}O	$^{15}N(p,n)^{15}O$	4	5.5-7.5	150
^{18}F	$^{18}O(p,n)^{18}F$	2.5	5-6	510

Conclusions and discussions about this study are listed as follows:

1. Accelerating protons seems to be the best choice to produce PET radioisotopes for the PET/MR system in LNMCB because there are conventional routes of production using accelerated protons for all the four desired short half-life PET isotopes ^{11}C, ^{13}N, ^{15}O e ^{18}F. Also, proton is a versatile option because it is able to produce a larger variety of PET radioisotopes. This is something positive because it allows the researchers to try to produce and carry out future experiments with other PET radioisotopes beyond the desired ones.

2. To guarantee the possibility of production of the desired PET isotopes (^{11}C, ^{13}N, ^{15}O e ^{18}F), the protons must be accelerated to kinetic energies at least higher than 6 MeV. At first sight, a good range of energy seems to be around 7 and 8 MeV. The next step to decide the energy would be to study the possible target geometries and perform irradiation simulations with beam energies within this range, in order to evaluate the production yields of different energies. It is important to consider any obstacle along the beam trajectory that could reduce its energy, for example, the thickness of the material that interfaces the vacuum chamber of the accelerator and the target, that can be a solid, liquid, or gaseous. These simulations would also serve to identify possible parasitic reactions.

3. For the production of radioisotopes, the higher the current, the more activity produced. But the beam current usually is a parameter limited by the accelerator. This parameter can be determined by the study of the accelerator design and is very important as an input for the yield simulations. Another point to be considered is that the PET isotope doses injected in small animals are much smaller than the ones injected in humans, for example. It means that the activity demands of our application are lower than conventional and, therefore, a lower current is not expected to be a major problem.

4. The analysis of the routes of production and activation cross-sections are important, yet more studies must be carried out about the feasibility of the production, in order to gather more details about the target, such as possible geometries, material availability and acquisition costs.

5. The nuclear reactions also produce ejecting particles. In the evaluated reactions, at least alpha particles and neutrons are expected to be emitted, but energetic photons will most certainly be produced too. Alpha particles have very low penetration power, but neutrons and gamma rays usually demand considerable radiation shielding. Therefore, simulations must be carried out to evaluate the shielding demands of each one of the possible target irradiation.

4 The High-frequency RFQ Linacs

CERN keeps a constant effort to positively impact society with the technology developed by their experts, actively searching for opportunities to transfer knowledge to other scientists and industries. To capitalise on the developments around the LINAC4 project [43], CERN created a study group to develop an RFQ to serve as injector of low energy beams in 3 GHz linac based proton-therapy facilities [44]. The project demanded compactness, and the solution proposed by CERN experts was to develop the first 750 MHz RFQ with a special beam optics design which allowed the accelerator to dismiss heavy radiation shielding. They noticed that their capability to develop small accelerators could serve as an important technology to solve other medical and industrial demands, resulting in the patent of the machining and beam optics design of this technology [23].

Other interesting application of a compact RFQ would be the production of PET radioisotopes, which is why CNPEM is considering to design a linac based on CERN's 750MHz RFQ to produce radioisotopes for the upcoming LNMCB. This chapter serves as a documentation of a bibliographical review of all published 750 MHz RFQ projects up to now. The purpose is to gather the publications of what has already been done and show where more information about the projects can be found. Learning from others projects will certainly help the engineers from CNPEM to carry out this project the best way possible.

The first publication about an RFQ working at 750 MHz is from 1997 by an Italian foundation called TERA (Fondazione per Adroterapia Oncologica), which has proposed an RFQ+DTL 7 MeV injector for a proton-therapy linac called TOP (Terapia Oncologica con Protoni) LINAC [45]. The idea was left aside due to technology limitations of the time, but revived by CERN experts in 2014. Publications about 750 MHz RFQ projects are presented in the next sections.

4.1 HF-RFQ for LIGHT by CERN/ADAM

The HF-RFQ (High Frequency RFQ) is a 750 MHz RFQ designed by CERN experts to be an injector for the 3 GHz proton-therapy linac of LIGHT (Linac for Image-Guided Hadron Therapy), which is a project headed by the Swiss company ADAM (Application of Detectors and Accelerators to Medicine). In 2014, the first publication [46] about this RFQ presented not only the challenges of development of such machine — a compact RFQ able to accelerate protons to 5 MeV —, but also preliminary ideas and sketches about the optimization of the accelerator transverse cross-section, beam dynamics, machining tests and the RF amplifier.

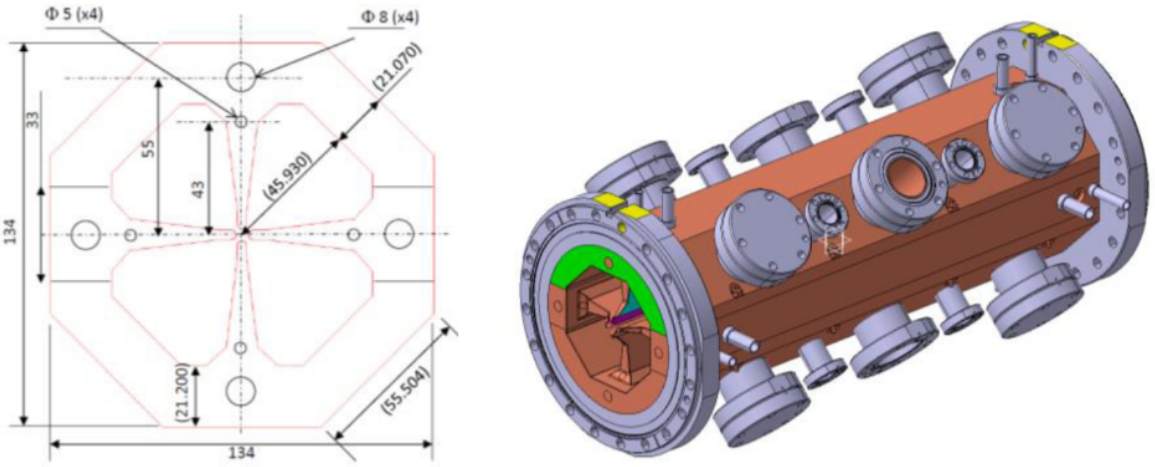

Figure 21 – Transverse cross section and CAD of a 50 cm module of the HF-RFQ. [46]

In 2015, the second publication about the HF-RFQ [44] shows more details of the beam dynamics design, like discussions about the chosen frequency in spite of other subharmonics of 3 GHz — 600 MHz and 1 GHz — and the detailed chosen solution, including the phase, aperture and modulation along the RFQ, in Figure 22, and also the full length of the linac, 2 meters.

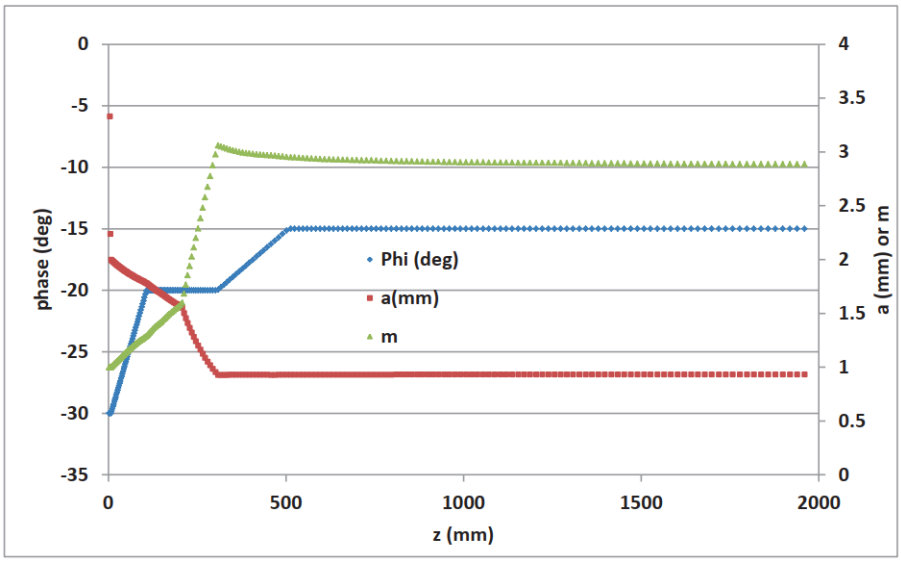

Figure 22 – Phase, aperture and modulation along the HF-RFQ for LIGHT project. [46]

The next publication in 2016 is not about an RFQ, but a DTL designed to work at 750 MHz [47]. This DTL, a IH (Inter-digital H) type in Figure 23, would receive the 5 MeV beam from the 750 MHz RFQ and accelerate it to 20 MeV, but no other publication about this design were found since then. In the same year, ADAM publishes a paper [48] about the LIGHT project, summarizing the status of the project as a whole. At that time, the design of the accelerator was ready and a first prototype was in construction.

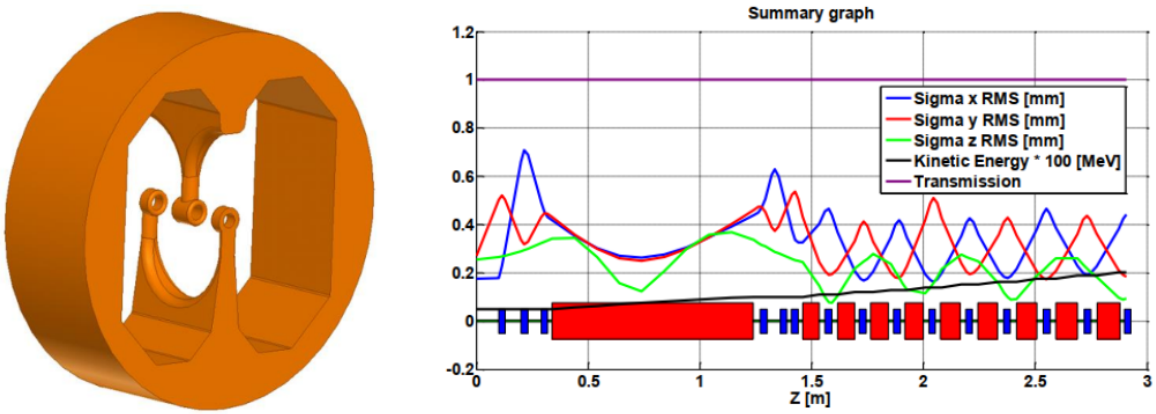

Figure 23 – Cell structure of the proposed 750 MHz IH DTL and graph of 3D envelopes, transmission and kinetic energy from RFQ output to 20 MeV. [47]

Still in 2016, CERN experts published about the 750 MHz RFQ they developed for LIGHT [49], reporting the successful machining of the cavity (Figure 24), RF measurements and overviewing the potential applications of 750 MHz RFQs for medicine and industry, such as the production of PET isotopes in hospitals, ion beam analysis, and acceleration of heavier ions with $q/m = 1/2$, for example, C^{6+}. The tuning of the resonating frequency of the HF-RFQ using bead pull measurements was then reported in 2017 [50].

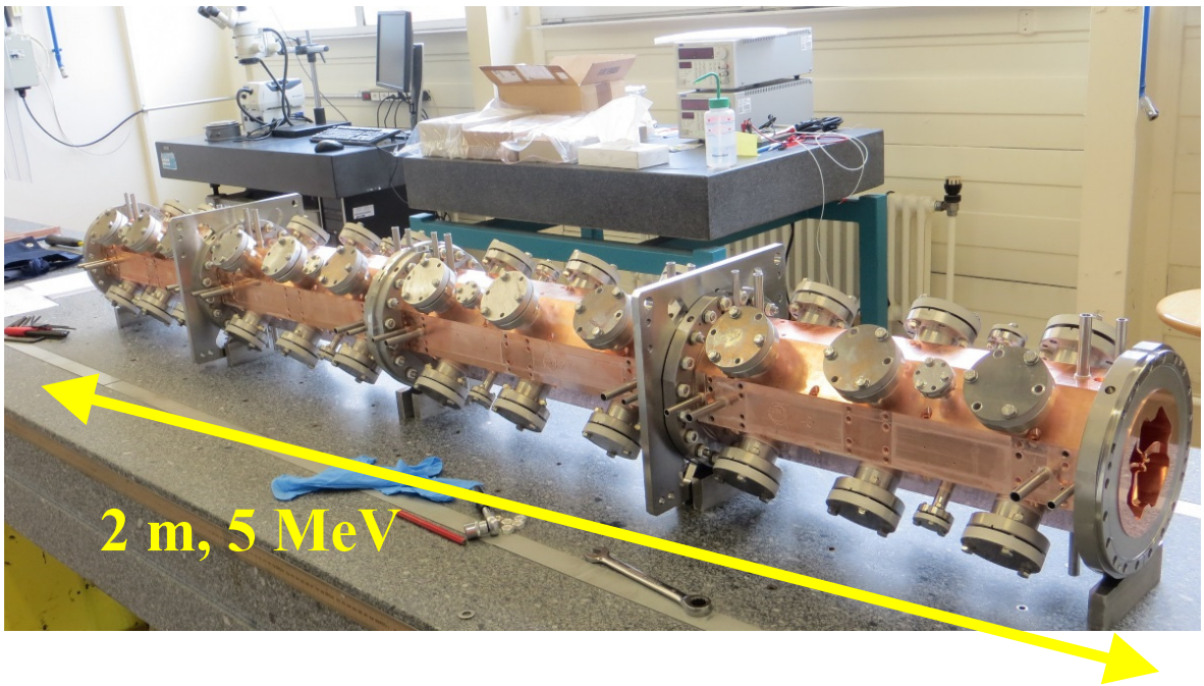

Figure 24 – Completely machined HF-RFQ for the project LIGHT. [49]

A new report about the successful beam commissioning of the HF-RFQ at ADAM test facility came out in 2018 [51]. In this paper, real measurements of the beam profile were compared to expected ones, like the transverse phase space plots of the beam after the RFQ in Figure 25. The results of the beam measurements of the HF-RFQ

were taken as reference for the higher energy sections of LIGHT, which had its status updated in the same year on the report [52].

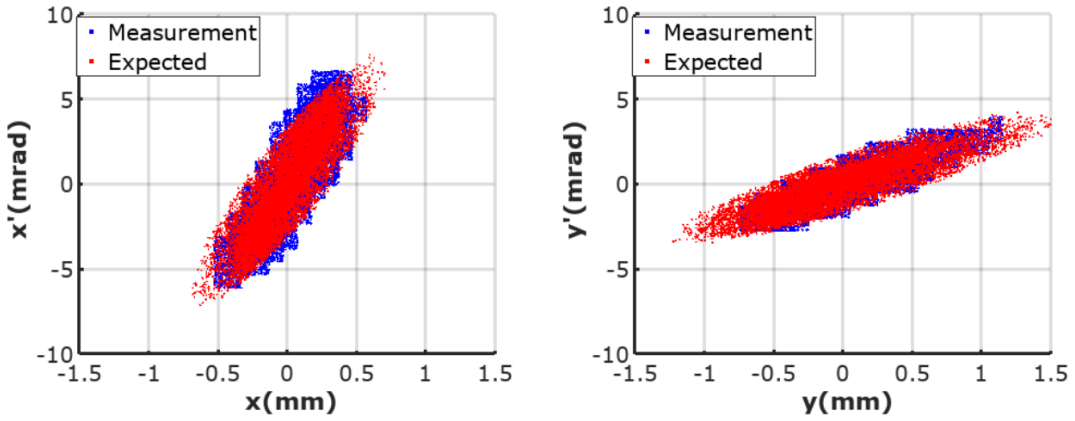

Figure 25 – Comparison of measured (blue) and expected (red) phase space plots of the beam after the RFQ. [51]

4.2 PIXE-RFQ for MACHINA Project by CERN/INFN

The PIXE-RFQ is a 1-meter-long 2 MeV proton 750 MHz RFQ designed to perform Proton Induced X-Ray Emission (PIXE) for cultural heritage material characterization. It was developed within the MACHINA (Movable Accelerator for Cultural Heritage *In-situ* Non-destructive Analysis) project to be the first transportable system for *in-situ* ion beam analysis, allowing employment in museums, or restoration centers. The RFQ design were adapted from the HF-RFQ to the requirements of PIXE analysis.

The PIXE-RFQ developed by CERN and INFN (Istituto Nazionale di Fisica Nucleare) brings innovative beam dynamics, sacrificing transmission in favor of short length and low power consumption, as reported in papers from 2018 and 2019 [53, 54]. These papers report the complete RF design, thermomechanical simulations and beam dynamics of the accelerator (Figure 27)

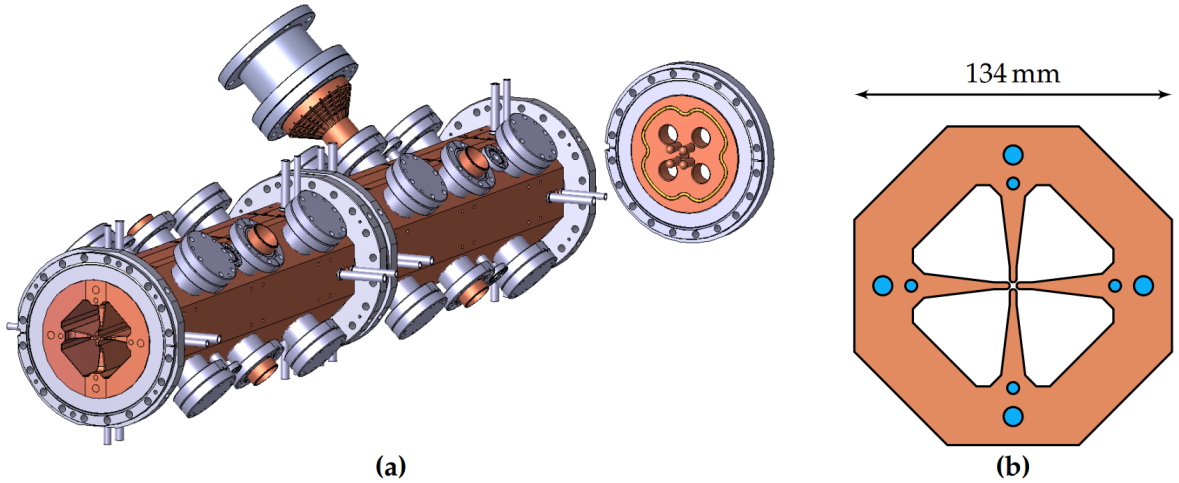

Figure 26 – (a) CAD model of the PIXE-RFQ, equipped with tuners, pumping ports, and coupler. (b) Cavity cross-section with water cooling channels. [53]

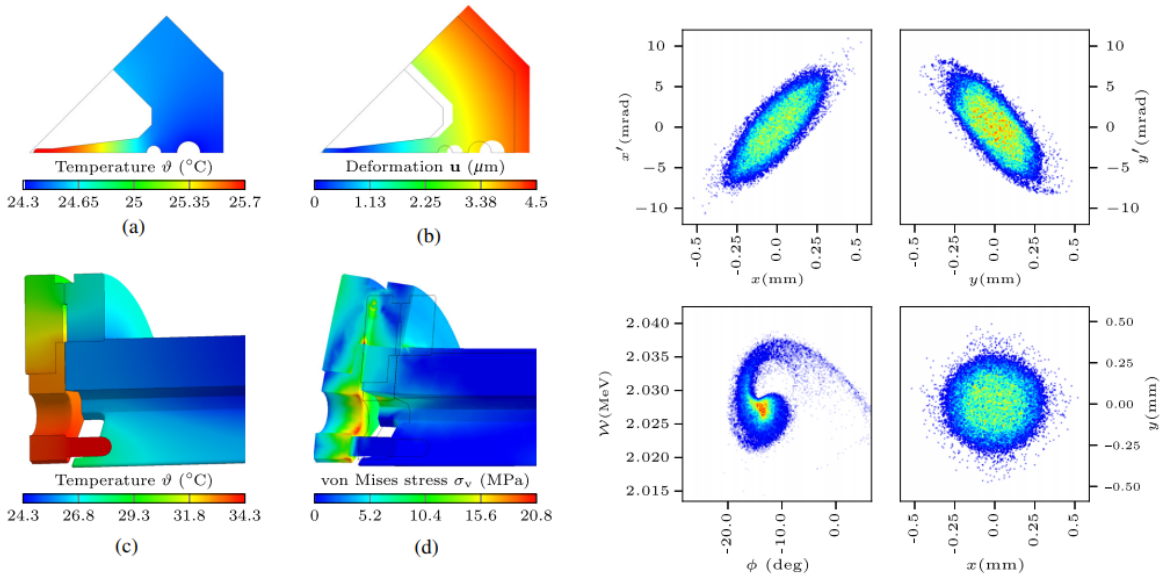

Figure 27 – Some thermal and phase space simulation results of PIXE-RFQ. The thermal simulations on the left side are for duty cycle $d = 2.5\%$, water temperature $\theta_w = 22°C$ and flow speed $v_w = 1m/s$: (a) and (c) show the resulting temperature distribution, while (b) and (d) are the corresponding deformation and equivalent stress. The phase spaces on the right side show the simulated output beam of the RFQ, which have a final energy of the bunch center at 2.028 MeV and phase of $-13.4°$. [54]

The 2019 paper [55] presents not only the detailed design and performances of the PIXE-RFQ, but also the fabrication technologies and status of the project. At the date, the cavities were machined and brazed, the RF tuning was about to start, vacuum systems and ion source were already tested, and beam test were planed for the end of 2019. Due to the COVID-19 pandemic, the project delayed, and the RF tuning of the PIXE-RFQ were only published in 2021 [56].

4.3 Carbon-RFQ for Bent Linac by CERN/CIEMAT

The Carbon-RFQ was designed as the first RF structure of a "bent linac" for carbon ion cancer therapy, Figure 28. This linac was conceived in the framework of a collaboration between CERN and CIEMAT (Centro de Investigaciones Energéticas, Medioambientales y Tecnológicas) with the key goal of improving the linac footprint such that it would fit better into a hospital facility. The complete proposed design of the Bent Linac is reported in [57].

The Carbon-RFQ, Figure 29, accelerates full stripped C^{6+} ions up to 5 MeV/u in a total length of 4.8 meters. This RFQ is also inspired by the HF-RFQ, but has several adaptations to match the application. The linac was subdivided in two fully decoupled RF cavities, referred and RFQ1 and RFQ2 (Figure 29). The gap between them are shown in Figure 30. Trapezoidal modulation of the vanes (Figure 31) were proposed and, according to the designers, it reduced the power consumption and length by 15%. The beam dynamics design of both sections are also shown in Figure 31. Until

2020, the Carbon-RFQ had a complete design, but was not yet machined. The authors intend to built the Carbon-RFQ to demonstrate the feasibility of the low-energy part of carbon ion therapy linacs, while ongoing studies are made to choose the accelerating structures subsequent to the Carbon-RFQ.

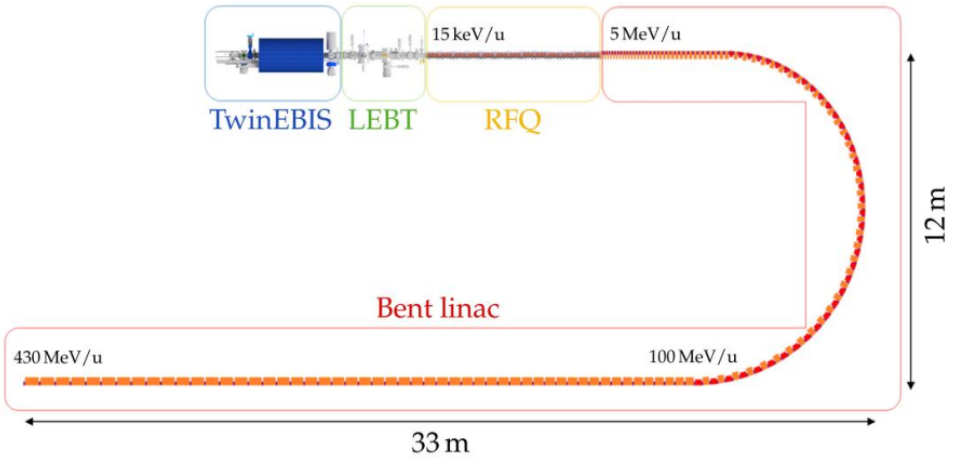

Figure 28 – Sketch of the Bent Linac accelerating structures footprint and respective energies. It consists of a ion source called TwinEBIS, a Low Energy Beam Transport (LEBT) section, the Carbon-RFQ and the bent section. [57]

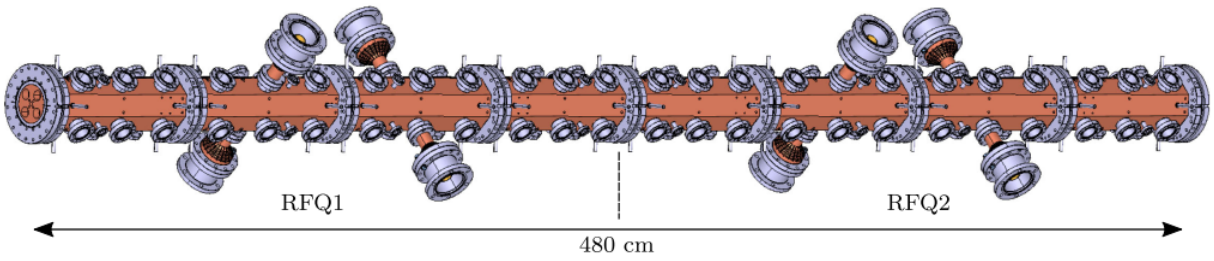

Figure 29 – CAD model of the two Carbon-RFQ cavities RFQ1 and RFQ2. Each cavity consists of four individually brazed 60cm modules, four input power couplers, 12 vacuum pumping ports, and 32 slug tuners. [58]

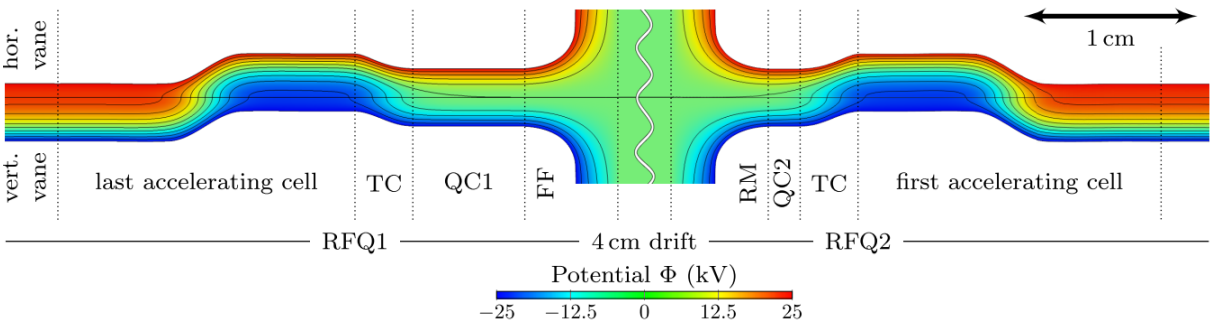

Figure 30 – Transfer path of the beam from the last accelerating cell of RFQ1 to the first accelerating cell of RFQ2. Both the horizontal and vertical plane are shown. A 4 cm separation was proved by simulations to be enough to decoupled the cavities. [58]

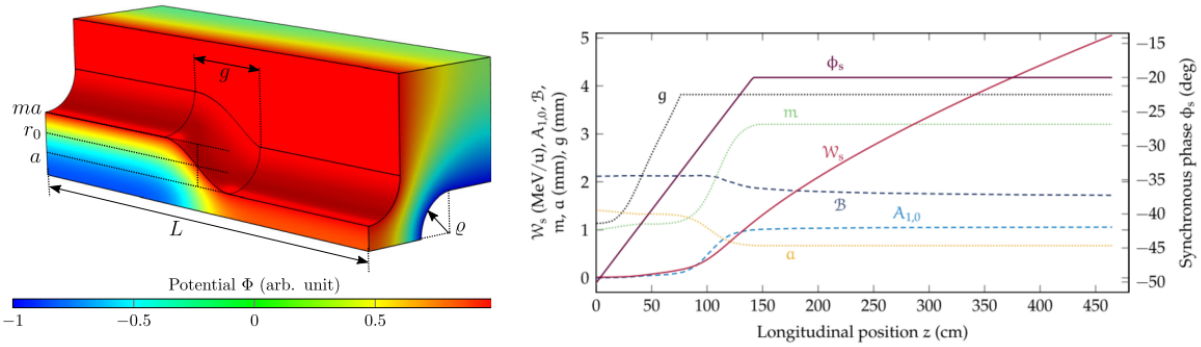

Figure 31 – (Left) Electric potential of the trapezoidal RFQ cell. Some geometrical parameters are shown, such as the aperture a, modulation m, the accelerating gap length g, and the cell length L. (Right) Beam dynamics parameters of the Carbon-RFQ with trapezoidal vanes: Synchronous phase ϕ_s, modulation m, aperture a, energy of the synchronous particle W_s, the quadrupole term $A_{0,1}$, the effective focusing force B, and the accelerating gap length g. [58]

4.4 RFQ for Linac 7 by UPV/TEKNIKER/Egile

The 2022 report [59] describes a 7 MeV compact linear proton accelerator project named LINAC 7 for low-current applications, that is being designed and built by Beam Laboratory of the University of the Basque Country (UPV/EHU) and the company Egile, all Spanish institutions. The accelerator consists of a proton source, which were already built and tested, a LEBT section followed by a 750 MHz RFQ and a DTL. The RFQ still in design phase, but is expected to accelerate proton up to 4 MeV along 1.5 m, capturing between 15% and 30% of the particles at the entrance. The vane modulation of the RFQ is not yet decided, but a cold model of one module was already machined in order to evaluate the quality of the machining. Figure 32 show photos of the RFQ cross-section and the assembled module. CERN experts are not involved in this project, such that this RFQ is not based on the original HF-RFQ, which was just an inspiration. In [60], the team describes in more details one of the expected applications of Linac7, the production of PET isotopes.

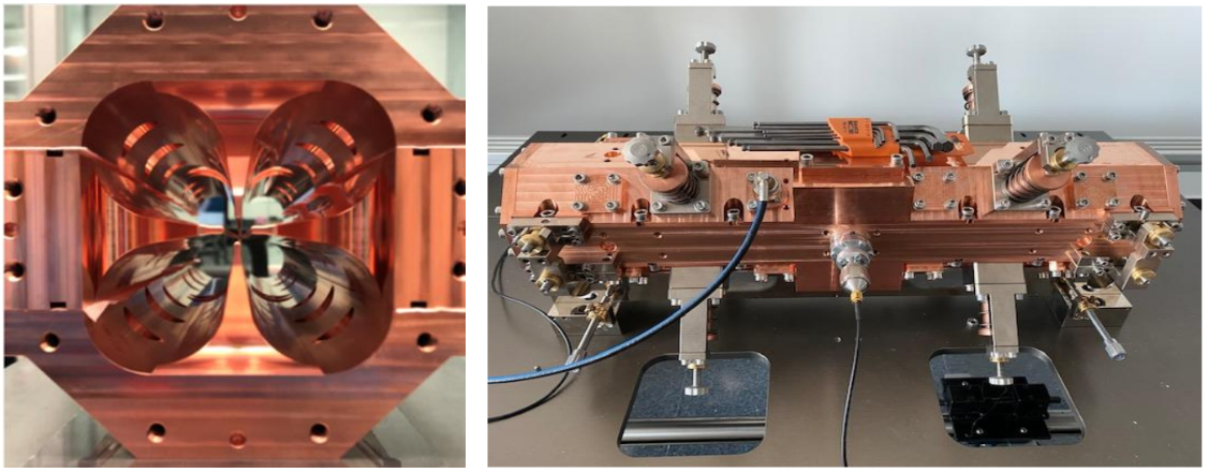

Figure 32 – Cross-section and module of the RFQ for Linac7. [60]

4.5 Conclusion

The bibliographic review resulted in the identification of four 750 MHz RFQ projects, that were presented in this chapter along with their available references. Table 3 summarizes essential information about each project.

Table 3 – Summary of 750 MHz RFQ projects.

750 MHz RFQ Projects	**HF-RFQ for LIGHT**	**PIXE-RFQ for MACHINA**	**Carbon-RFQ for Bent Linac**	**RFQ for Linac7**
Ion	H^+	H^+	C^{6+}	H^+
Output Energy	5 MeV	2 MeV	5 MeV/u	4 MeV
Length	2 m	1 m	4.8 m	1.5 m
Application	Injector for proton therapy linac	PIXE analysis of cultural heritage	Injector for carbon ion therapy linac	Low-current applications
Status	Output beam Measured	RF tuned	Designed and Simulated	In design
References	[46, 44, 47, 48, 49, 50, 52, 51]	[53, 55, 30, 56]	[57, 58, 30]	[59, 60]

Besides the novel and high frequency of 750 MHz, one can notice that the output energy of these RFQs are higher than the traditional RFQs, which were first developed to accelerate ions to not more than $\beta = 0.06$, corresponding to protons with around 1.65 MeV. We see that the evolution of accelerator's technology, like higher precision machining and novel RF sources, allowed RFQs to work at higher frequencies and, therefore, accelerate to higher energies in shorter lengths. The presented projects are certainly the first examples of a new generation of linacs, which are compact enough to, for example, fit inside hospitals or be transportable, bringing new medical and industrial solutions to humanity.

5 General Conclusion

The present thesis documented preliminary studies for the development of a compact linear accelerator that will locally produce short half-life PET radioisotopes for the study of dangerous pathogens in small animals using a hybrid PET/MR imaging system inside the first Latin American BLS-4 laboratory LNMCB under construction at CNPEM. In the framework of a collaboration agreement, CERN experts proposed a solution based on an HF-RFQ. The thesis properly summarized the initial efforts that CNPEM has made to start this project, despite the fact that the technological challenges of this kind of project are far beyond of what would fit in a bachelor's thesis. A research for the routes of production of the short half-life PET radioisotopes ^{11}C, ^{13}N, ^{15}O and ^{18}F showed that proton seems to be the best bombarding particle because there already exists conventional routes of production using protons as bombarding particle for all the desired radioisotopes. Then, a brief analysis of the cross-section curves for the identified routes of production concluded that at least more than 6 MeV of kinetic energy per proton is necessary to guarantee the production of all four of them. This analysis also identified that an optimal output energy of the accelerator would be between 7 and 8 MeV. Yet, simulations must be carried out to confirm these conclusions and identify other possibles problems, like parasitic reactions that could disturb the expected production. Moreover, a bibliographic review of all four existing HF-RFQ projects were presented. This review not only gathered all the available references about these projects, but also identified basic information, such as the accelerated ion, RFQ output energy, length of RFQ cavity, application, and status of each project.

References

1 Meechan, Paul J and Potts, Jeffrey. Biosafety in microbiological and biomedical laboratories - 6th Edition. Centers for Disease Control and Prevention, National Institutes of Health, 2020–06. Cited on page 1.

2 Fundação Oswaldo Cruz. *Nível de Biossegurança 4 (NB-4)*. Available in: <http://www.fiocruz.br/biosseguranca/Bis/lab_virtual/nb4.html>. Accessed: 2022-08-22. Cited on page 1.

3 Agência Brasil. *Ministro defende construção de laboratório de biossegurança máxima: Marcos Pontes disse que local escolhido é Campinas, em São Paulo*. 2021–05–18. Available in: <https://agenciabrasil.ebc.com.br/geral/noticia/2021-05/ministro-defende-construcao-de-laboratorio-de-biosseguranca-maxima>. Accessed: 2022-08-22. Cited on page 1.

4 Global Bio Labs Project. *Mapping BSL-4s around the world*. <https://www.globalbiolabs.org/map>. Accessed: 2022-08-22. Cited on page 1.

5 WADSAK, W.; MITTERHAUSER, M. Basics and principles of radiopharmaceuticals for PET/CT. *European journal of radiology*, Elsevier, v. 73, n. 3, p. 461–469, 2010. Cited 2 times on pages 1 and 28.

6 BRITO, M. F. de A. *Sistema PET/MR híbrido: Aplicação para imageamento in vivo em ambiente de máxima biocontenção*. 2022. Engineering Physics Bachelor's Thesis available in: <https://repositorio.ufscar.br/handle/ufscar/16035?show=full>. Cited on page 1.

7 Comunicação CNPEM. *CNPEM e CERN firmam acordo de colaboração*. 2020–12–04. Available in: <https://cnpem.br/cnpem-e-cern-firmam-acordo-de-colaboracao/>. Accessed: 2022-08-22. Cited on page 1.

8 CHERRY, S. R.; SORENSON, J. A.; PHELPS, M. E. *Physics in nuclear medicine*. [S.l.]: Elsevier Health Sciences, 2012. Cited 3 times on pages 2, 11, and 13.

9 World Nuclear Association. *The Many Uses of Nuclear Technology*. 2021–05. Available in: <https://world-nuclear.org/information-library/non-power-nuclear-applications/overview/the-many-uses-of-nuclear-technology.aspx>. Accessed: 2022-08-22. Cited on page 2.

10 RUTH, T. J. The Medical Isotope Crisis: How We Got Here and Where We Are Going. *Journal of Nuclear Medicine Technology*, Society of Nuclear Medicine, v. 42, n. 4, p. 245–248, 2014, <https://tech.snmjournals.org/content/42/4/245>. ISSN 0091-4916. Cited on page 2.

11 NOORDEN, R. V. Radioisotopes: The medical testing crisis. *Nature*, Nature Publishing Group, v. 504, n. 7479, p. 202, 2013. Cited on page 2.

12 IBA. *Cyclone® IKON - Compact & industrial high energy cyclotron for large production of PET and SPECT isotopes.* 2022–08–22. <https://www.iba-radiopharmasolutions.com/cyclone-ikon>. Cited on page 3.

13 IBA. *Cyclone® IKON by IBA - Ready to accelerate into the future?* Visited in: 2022–08–22. <https://www.iba-radiopharmasolutions.com/sites/default/files/2021-08/CycloneIKONFinalR01_LD.pdf>. Cited on page 3.

14 O'BRIEN, H. A. Accelerator preparation of radioisotopes for medical applications. v. 33, 1979–11. Cited on page 4.

15 MAUSNER, L. F.; RICHARDS, P. The Production of Spallation Radionuclides for Medical Applications at BLIP. *IEEE Transactions on Nuclear Science*, v. 30, n. 2, p. 1793–1796, 1983. Cited on page 4.

16 COMASTRA, D.; CGRP, N. E. N.; GEOMETRY, L. Accelerating structure parameters of the New England Nuclear Corp. proton linac. In: *Proc. 1979 Linear Accelerator Conf., BNL*. [S.l.: s.n.], 1979. v. 51134, p. 32. Cited on page 4.

17 BENTLEY, R. New England Nuclear Corp. Linear Accelerator Progress Report. In: *Proc. 1981 Linear Accelerator Conference*. [S.l.: s.n.], 1981. p. 349. Cited on page 4.

18 HAMM, R. et al. A compact proton linac for positron tomography. In: *1986 Linear Accelerator Conference Proceedings*. [S.l.: s.n.], 1986. p. 141–143. Cited 2 times on pages 4 and 5.

19 AccSys Technology Inc. *PULSAR® - PET Isotope Production Systems*. Visited in: 2022–08–22. <https://www.accsys.com/pulsar.html>. Cited on page 4.

20 AccSys Techonology Inc. *Mobile PET Isotope Production Lab*. Visited in 2022–08–22. <https://www.accsys.com/pdf/pulsar_mob.pdf>. Cited on page 5.

21 POTTER, J. M. A parallel planar triode array high power RF system for accelerator applications. 1990. Cited on page 5.

22 CERN Knowledge Transfer. *High Frequency Compact Linear Proton Accelerator*. Visited in: 2022–08–29. <https://knowledgetransfer.web.cern.ch/technologies/high-frequency-compact-linear-proton-accelerator>. Cited on page 6.

23 LOMBARDI, A. et al. *High frequency compact low-energy linear accelerator design*. [S.l.]: Google Patents, 2018. US Patent 10,051,721. Cited 2 times on pages 6 and 31.

24 WANGLER, T. P. *RF Linear accelerators*. [S.l.]: John Wiley & Sons, 2008. Cited 6 times on pages 11, 15, 16, 20, 23, and 24.

25 WEISS, M. *Radio-frequency quadrupole*. [S.l.], 1987. Cited 3 times on pages 11, 19, and 20.

26 RUTHERFORD, E. Radium standards and nomenclature. *Nature*, v. 84, n. 2136, p. 430–431, 1910. Cited on page 12.

27 ÜBER ein neues Prinzip zur Herstellung hoher Spannungen. Cited on page 14.

28 KAPCHINSKII, I. M.; TEPLYAKOV, V. A. LINEAR ION ACCELERATOR WITH SPATIALLY HOMOGENEOUS STRONG FOCUSING. *Instrum. Exp. Tech. (USSR) (Engl. Transl.) No. 2, 322-6 (Mar-Apr 1970)*. <https://www.osti.gov/biblio/4032849>. Cited on page 19.

29 KAPCHINSKII, I. M.; TEPLYAKOV, V. A. POSSIBILITY OF REDUCING THE INJECTION ENERGY AND INCREASING THE LIMIT CURRENT IN AN ION LINEAR ACCELERATOR. *Instrum. Exp. Tech. (USSR) (Engl. Transl.) No. 4, 973-5 (Jul-Aug 1970).* <*https://www.osti.gov/biblio/4055271*>. Cited on page 19.

30 POMMERENKE, H. W. Compact radio-frequency quadrupoles for industrial and medical applications - PhD Thesis. Universität Rostock, 2020, <http://rosdok.uni--rostock.de/resolve/id/rosdok_disshab_0000002457>. Cited 3 times on pages 20, 22, and 38.

31 TÁRKÁNYI, F. et al. Recommended nuclear data for medical radioisotope production: diagnostic positron emitters. *Journal of Radioanalytical and Nuclear Chemistry*, Springer, v. 319, n. 2, p. 533–666, 2019. <https://www–nds.iaea.org/medical/>. Cited 3 times on pages 25, 27, and 28.

32 WANG, Y. et al. Production Review of Accelerator-Based Medical Isotopes. *Molecules*, Multidisciplinary Digital Publishing Institute, v. 27, n. 16, p. 5294, 2022. Cited on page 25.

33 QAIM, S. M. et al. Charged-particle cross section database for medical radioisotope production. *Journal of Nuclear Science and Technology*, Taylor & Francis, v. 39, n. sup2, p. 1282–1285, 2002. Cited on page 26.

34 MILLER, P. W. et al. Synthesis of 11C, 18F, 15O, and 13N radiolabels for positron emission tomography. *Angewandte Chemie International Edition*, Wiley Online Library, v. 47, n. 47, p. 8998–9033, 2008. Cited on page 26.

35 PICHLER, V. et al. An overview of PET radiochemistry, part 1: the covalent labels 18F, 11C, and 13N. *Journal of Nuclear Medicine*, Soc Nuclear Med, v. 59, n. 9, p. 1350–1354, 2018. Cited on page 26.

36 ALMUHAIDEB, A.; PAPATHANASIOU, N.; BOMANJI, J. 18F-FDG PET/CT imaging in oncology. *Annals of Saudi medicine*, King Faisal Specialist Hospital & Research Centre, v. 31, n. 1, p. 3–13, 2011. Cited on page 26.

37 CHÉTELAT, G. et al. Amyloid-PET and 18F-FDG-PET in the diagnostic investigation of Alzheimer's disease and other dementias. *The Lancet Neurology*, Elsevier, v. 19, n. 11, p. 951–962, 2020. Cited on page 26.

38 QIN, C. et al. 18F-FDG PET/CT findings of COVID-19: a series of four highly suspected cases. *European journal of nuclear medicine and molecular imaging*, Springer, v. 47, n. 5, p. 1281–1286, 2020. Cited on page 26.

39 LÅNGSTRÖM, B.; ITSENKO, O.; RAHMAN, O. [11C] Carbon monoxide, a versatile and useful precursor in labelling chemistry for PET-ligand development. *Journal of Labelled Compounds and Radiopharmaceuticals: The Official Journal of the International Isotope Society*, Wiley Online Library, v. 50, n. 9-10, p. 794–810, 2007. Cited on page 26.

40 LODI, F. et al. Synthesis of oncological [11C] radiopharmaceuticals for clinical PET. *Nuclear medicine and biology*, Elsevier, v. 39, n. 4, p. 447–460, 2012. Cited on page 26.

41 XIANGSONG, Z. et al. Usefulness of 13N-NH3 PET in the evaluation of brain lesions that are hypometabolic on 18F-FDG PET. *Journal of neuro-oncology*, Springer, v. 105, n. 1, p. 103–107, 2011. Cited on page 27.

42 YORIMITSU, H. et al. Ultra-rapid synthesis of 15O-labeled 2-deoxy-D-glucose for positron emission tomography (PET). *Angewandte Chemie International Edition*, Wiley Online Library, v. 44, n. 18, p. 2708–2711, 2005. Cited on page 28.

43 ROSSI, C. et al. *Commissioning and Operational Experience Gained with the Linac4 RFQ at CERN*. [S.l.], 2014. Cited on page 31.

44 LOMBARDI, A. et al. *Beam dynamics in a high frequency RFQ*. [S.l.], 2015. Cited 3 times on pages 31, 32, and 38.

45 PICARDI, L.; RONSIVALLE, C.; VIGNATI, A. The ISS Protontherapy Linac. In: AMERICAN INSTITUTE OF PHYSICS. *AIP Conference Proceedings*. [S.l.], 1997. v. 392, n. 1, p. 1249–1252. Cited on page 31.

46 VRETENAR, M. et al. *A compact high-frequency RFQ for medical applications*. [S.l.], 2014. Cited 3 times on pages 31, 32, and 38.

47 BENEDETTI, S. et al. Design of a 750 MHz IH structure for medical applications. In: *Proc. of Linear Accelerator Conference-LINAC16*. [S.l.: s.n.], 2016. Cited 3 times on pages 32, 33, and 38.

48 DEGIOVANNI, A. et al. LIGHT: a linear accelerator for proton therapy. *Proceedings of NAPAC2016, Chicago, USA*, 2016. Cited 2 times on pages 32 and 38.

49 VRETENAR, M. et al. High-frequency compact RFQs for medical and industrial applications. In: *inProc. 28th Linear Accelerator Conf.(LINAC'16), East Lansing, MI, USA*. [S.l.: s.n.], 2016. Cited 2 times on pages 33 and 38.

50 KOUBEK, B. et al. Tuning of the CERN 750 MHz RFQ for medical applications. In: *Proc. 28th Linear Accelerator Conf.(LINAC'16)*. [S.l.: s.n.], 2016. Cited 2 times on pages 33 and 38.

51 DIMOV, V. et al. Beam commissioning of the 750 MHz proton RFQ for the LIGHT prototype. In: *9th International Particle Accelerator Conference (IPAC2018), Vancouver, BC, Canada, JACoW, Geneva, Switzerland*. [S.l.: s.n.], 2018. p. 658–660. Cited 3 times on pages 33, 34, and 38.

52 DEGIOVANNI, A. et al. Status of the Commissioning of the LIGHT Prototype. In: JACOW PUBLISHING, GENEVA, SWITZERLAND. *9th Int. Particle Accelerator Conf.(IPAC'18), Vancouver, BC, Canada, April 29-May 4, 2018*. [S.l.], 2018. p. 425–428. Cited 2 times on pages 34 and 38.

53 POMMERENKE, H. et al. RF Design of a High-frequency RFQ Linac for PIXE Analysis. In: *Proceedings of the 29th Linear Accelerator Conference (LINAC2018)*. [S.l.: s.n.], 2018. p. 822–825. Cited 2 times on pages 34 and 38.

54 POMMERENKE, H. W. et al. rf design studies on the 750 MHz radio frequency quadrupole linac for proton-induced x-ray emission analysis. *Physical Review Accelerators and Beams*, APS, v. 22, n. 5, p. 052003, 2019. Cited 2 times on pages 34 and 35.

55 MATHOT, S. et al. The CERN PIXE-RFQ, a transportable proton accelerator for the machina project. *Nuclear Instruments and Methods in Physics Research Section B: Beam Interactions with Materials and Atoms*, Elsevier, v. 459, p. 153–157, 2019. Cited 2 times on pages 35 and 38.

56 POMMERENKE, H. W.; RIENEN, U. van; GRUDIEV, A. rf measurements and tuning of the 1-m-long 750 MHz radio-frequency quadrupole for artwork analysis. *Nuclear Instruments and Methods in Physics Research Section A: Accelerators, Spectrometers, Detectors and Associated Equipment*, Elsevier, v. 1011, p. 165564, 2021. Cited 2 times on pages 35 and 38.

57 BENCINI, V. *Design of a novel linear accelerator for carbon ion therapy*. Tese (Doutorado) — Rome U., 2020. Cited 3 times on pages 35, 36, and 38.

58 BENCINI, V. et al. 750 MHz radio frequency quadrupole with trapezoidal vanes for carbon ion therapy. *Physical Review Accelerators and Beams*, APS, v. 23, n. 12, p. 122003, 2020. Cited 3 times on pages 36, 37, and 38.

59 FEUCHTWANGER, J. et al. New Generation Compact Linear Accelerator for Low-Current, Low-Energy Multiple Applications. *Applied Sciences*, MDPI, v. 12, n. 9, p. 4118, 2022. Cited 2 times on pages 37 and 38.

60 ETXEBARRIA, V. et al. Manufacturing of Radiopharmaceutical Isotopes through the LINAC 7 Accelerator For Biomedical Applications. *Dyna Acelerado*, v. 7, 2022. Cited 2 times on pages 37 and 38.